JBC RESEARCH ARTICLE

Active site architecture of an acetyl xylan esterase indicates a novel cold adaptation strategy

Received for publication, January 18, 2021, and in revised form, May 20, 2021 Published, Papers in Press, May 28, 2021,
https://doi.org/10.1016/j.jbc.2021.100841

Yi Zhang[1,2,3,‡], **Hai-Tao Ding**[4,‡], **Wen-Xin Jiang**[1], **Xia Zhang**[5], **Hai-Yan Cao**[1], **Jing-Ping Wang**[1], **Chun-Yang Li**[2,3], **Feng Huang**[1], **Xi-Ying Zhang**[1], **Xiu-Lan Chen**[1], **Yu-Zhong Zhang**[2,3,6,*], and **Ping-Yi Li**[1,*]

From the [1]State Key Laboratory of Microbial Technology, Shandong University, Qingdao, China; [2]College of Marine Life Sciences, and Frontiers Science Center for Deep Ocean Multispheres and Earth System, Ocean University of China, Qingdao, China; [3]Laboratory for Marine Biology and Biotechnology, Pilot National Laboratory for Marine Science and Technology, Qingdao, China; [4]SOA Key Laboratory for Polar Science, Polar Research Institute of China, Shanghai, China; [5]Department of Molecular Biology, Qingdao Vland Biotech Inc, Qingdao, China; [6]State Key Laboratory of Microbial Technology, Marine Biotechnology Research Center, Shandong University, Qingdao, China

Edited by Gerald Hart

SGNH-type acetyl xylan esterases (AcXEs) play important roles in marine and terrestrial xylan degradation, which are necessary for removing acetyl side groups from xylan. However, only a few cold-adapted AcXEs have been reported, and the underlying mechanisms for their cold adaptation are still unknown because of the lack of structural information. Here, a cold-adapted AcXE, *Al*AXEase, from the Arctic marine bacterium *Arcticibacterium luteifluviistationis* SM1504^T was characterized. *Al*AXEase could deacetylate xylooligosaccharides and xylan, which, together with its homologs, indicates a novel SGNH-type carbohydrate esterase family. *Al*AXEase showed the highest activity at 30 °C and retained over 70% activity at 0 °C but had unusual thermostability with a T_m value of 56 °C. To explain the cold adaption mechanism of *Al*AXEase, we next solved its crystal structure. *Al*AXEase has similar noncovalent stabilizing interactions to its mesophilic counterpart at the monomer level and forms stable tetramers in solutions, which may explain its high thermostability. However, a long loop containing the catalytic residues Asp200 and His203 in *Al*AXEase was found to be flexible because of the reduced stabilizing hydrophobic interactions and increased destabilizing asparagine and lysine residues, leading to a highly flexible active site. Structural and enzyme kinetic analyses combined with molecular dynamics simulations at different temperatures revealed that the flexible catalytic loop contributes to the cold adaptation of *Al*AXEase by modulating the distance between the catalytic His203 in this loop and the nucleophilic Ser32. This study reveals a new cold adaption strategy adopted by the thermostable *Al*AXEase, shedding light on the cold adaption mechanisms of AcXEs.

Acetyl xylan esterases (AcXEs) (EC 3.1.1.72) are a kind of carbohydrate esterases (CEs) that hydrolyze ester bonds to liberate acetic acid from acetylated hemicellulose, typically xylans and xylooligosaccharides (1). AcXEs are widely distributed in bacteria, fungi, plants, and mammals (1). Microbial AcXEs are capable of facilitating the access of main-chain depolymerizing enzymes to xylan (2), thereby playing an important role in terrestrial and marine xylan degradation and recycling.

Based on amino acid similarities, microbial AcXEs fall into nine families, CE families 1 to 7, 12, and 16 (3), as well as a novel CE family (the Axe2 family) recently proposed based on the studies of two AcXEs, Axe2 and Cbes-AcXE2 (4, 5). Although some AcXEs are found only to deacetylate xylooligosaccharides (5, 6), most AcXEs are reported to be active on both acetyl xylan and acetylated xylooligosaccharides (1, 4). In addition to the hydrolysis of acetylated xylooligosaccharides, many AcXEs are also capable of hydrolyzing other acetylated oligosaccharides/monosaccharides with relatively high activities, especially for the acetylated glucose (7–9). Except for those from families CE1, CE4, CE5, and CE7, AcXEs from the other CE families also belong to the SGNH hydrolase subfamily of the GDSL family (1, 4). GDSL family esterases are characterized by the nucleophilic serine located in the conserved GDSL motif rather than in the canonical GxSxG motif reported in other serine esterases (10). Some of the GDSL enzymes are further classified into the SGNH hydrolase subfamily because of the presence of four strictly conserved active site residues Ser, Gly, Asn, and His in the four conserved blocks I, II, III, and V, respectively (11, 12). The SGNH hydrolase adopts a three-layered αβα sandwich-like fold (10, 13). Among the SGNH-type AcXEs, only structures of the AcXEs from families CE2, CE3, and CE6, and the Axe2 family have been reported. Structural analyses reveal that AcXEs from CE3, CE6, and the Axe2 family possess a typical SGNH hydrolase fold with a standard Ser-His-Asp catalytic triad (1, 14, 15), whereas members from CE2 are bidomain enzymes, containing an N-terminal β-sheet domain and a C-terminal SGNH-hydrolase domain, and generally have a Ser-His catalytic diad (1, 16).

For the SGNH-type AcXEs, while most characterized enzymes are mesophilic or thermophilic, which usually originate from warm terrestrial environments (4, 5, 17), AxeA from the anaerobic rumen fungus *Orpinomyces* sp. strain PC-2 has been

‡ These authors contributed equally to this work.
* For correspondence: Ping-Yi Li, lipingyipeace@sdu.edu.cn; Yu-Zhong Zhang, zhangyz@sdu.edu.cn.

reported to be cold adapted (18). AxeA efficiently deacetylates acetylated xylan at low temperatures of 15 to 30 °C (18). However, owing to the lack of structural information, the underlying mechanisms for the cold adaptation of AcXEs are still unknown by far.

Cold-adapted enzymes help their source strains to adapt to extremely cold environments. Compared with mesophilic/thermophilic homologs, cold-adapted enzymes display higher catalytic activity at low temperatures because of their more flexible structures (19, 20). Most cold-adapted enzymes show a global rather than uniform distribution of their flexibility throughout the whole structure, therefore resulting in their low thermostability (21). However, some cold-adapted enzymes are also reported to have unusual thermal stability, such as the vibriolysin E495 from an Arctic sea ice bacterium (22), the phenylalanine hydroxylase *Cp*PAH from *Colwellia psychrerythraea* 34H (23), and the isocitrate dehydrogenase *Dp*IDH from *Desulfotalea psychrophila* (24). Compared with its mesophilic homologs, E495 has similar noncovalent stabilizing interactions but higher flexibility because of the reduction of hydrogen-bond stability in the dynamic structure, suggesting the optimization of hydrogen-bonding dynamics as a strategy for cold adaptation of enzymes (22). For *Cp*PAH and *Dp*IDH, both enzymes have local flexibility around their active sites, which leads to their cold adaptation without compromising the global stability of proteins (23, 24). Thus, cold-active enzymes may have diverse cold adaption strategies, and the cold adaption mechanisms for other enzymes, especially for the SGNH-type AcXEs, need to be further explored.

Arcticibacterium luteifluviistationis SM1504^T is a cold-adapted bacterium isolated from an Arctic surface seawater sample from King's Fjord, Svalbard (25, 26). Here, we identified and characterized a novel SGNH-type AcXE, *Al*AXEase, from strain SM1504^T, which, together with its homologs, represents a new SGNH-type CE family. *Al*AXEase deacetylated xylooligosaccharides and acetyl xylan. Biochemical characterization showed that *Al*AXEase is a cold-adapted enzyme with high thermostability. We further solved the crystal structure of *Al*AXEase to probe the structural basis for its cold adaptation. Structural and enzyme kinetic analyses combined with molecular dynamics (MD) simulations of WT *Al*AXEase and its mutant E190A at different temperatures revealed that *Al*AXEase has a long and flexible catalytic loop around its active site that contributes to the cold adaptation of *Al*AXEase by modulating the distance between the catalytic His203 in this loop and the nucleophilic Ser32.

Results

*Al*AXEase belongs to a novel SGNH-type CE family

A gene encoding a GDSL family protein (GenBank Accession No. WP_111370902) was obtained from the genome sequence of the marine cold-adapted bacterium *A. luteifluviistationis* SM1504^T based on gene annotation, which was designated as *AlAXEase*. *AlAXEase* is 669 bp in length, encoding a putative lipolytic enzyme of 222 amino acid residues. Based on the SignalP 5.0 prediction, *Al*AXEase contains an N-terminal signal peptide sequence (14 residues in length).

*Al*AXEase shows the highest sequence identity (66%) to an uncharacterized GDSL family protein from *Emticicia aquatilis* (GenBank Accession No. WP_188769581). Among all the characterized GDSL enzymes, *Al*AXEase is most closely related to the SGNH-type acetyl xylan esterase Axe2 from *Geobacillus stearothermophilus* (4), with a low sequence identity of 24%, suggesting that *Al*AXEase is a potential novel SGNH-type CE. To reveal the relationship between *Al*AXEase and other CEs, a phylogenetic tree was constructed, including *Al*AXEase and its homologs, Axe2 and its homologs, and characterized enzymes from known SGNH-type CE families 2, 3, 6, 12, and 16 (Fig. 1). The tree showed that *Al*AXEase and its homologs are clustered as a separate group from all other characterized SGNH-type CEs (Fig. 1). Based on these data, we suggest that *Al*AXEase and its homologs represent a new SGNH-type CE family.

Multiple sequence alignment showed that *Al*AXEase contains the four characteristic sequence blocks of SGNH hydrolases, blocks I, II, III, and V (Fig. 2), further supporting that *Al*AXEase is a SGNH hydrolase. *Al*AXEase has a catalytic triad possibly formed by Ser32, Asp200, and His203 (Fig. 2). The catalytic Ser32 is located in the conserved GDSxT motif (block I) close to the N terminus, while Asp200 and His203 are located in the conserved DxxHL(P) motif (block V) (Fig. 2). Residues Gly69 and Asn98 were predicted to be involved in the oxyanion hole, which are located in blocks II and III, respectively (Fig. 2).

*Al*AXEase is a cold-adapted acetyl xylan esterase with unusual thermostability

*Al*AXEase without the predicted signal peptide was overexpressed in *Escherichia coli* BL21 (DE3) with the coexpression of the chaperone protein *gro*ES-*gro*EL and purified. The recombinant *Al*AXEase with a calculated molecular mass of 23.5 kDa could hydrolyze *p*-nitrophenyl acetate (*p*NPC2), 1-napthyl acetate, and phenyl acetate but showed no detectable activity against *p*NP-acylesters with an acyl chain length of more than two carbon atoms (Table 1), suggesting that *Al*AXEase may have a small substrate-binding pocket. Using *p*NPC2 as the substrate, *Al*AXEase exhibited the highest activity at 30 °C and retained more than 70% of the highest activity at 0 °C (Fig. 3*A*), indicating that it is a cold-adapted enzyme. However, *Al*AXEase displayed unexpected tolerance to heat treatment, retaining 75% of the highest activity at 50 °C and 45% at 60 °C after 1 h incubation (Fig. 3*B*). Moreover, *Al*AXEase had a relatively high T_m value of 56 °C (Fig. 3*C*). These results indicate that the cold-adapted *Al*AXEase has unusual thermal stability. The cold-adapted *Al*AXEase was also resistant to mechanic stirring (Fig. S1). *Al*AXEase exhibited the highest activity at pH 9.0 and was stable in a range of pH 5.0 to 11.0 (Fig. 3*D* and Fig. S2). *Al*AXEase is also a halotolerant enzyme, whose activity was not influenced by 3.0 M NaCl (Fig. 3*E*). Among all the tested metal ions, only 10 mM of Cu^{2+}, Fe^{2+}, or Fe^{3+} severely inhibited *Al*AXEase

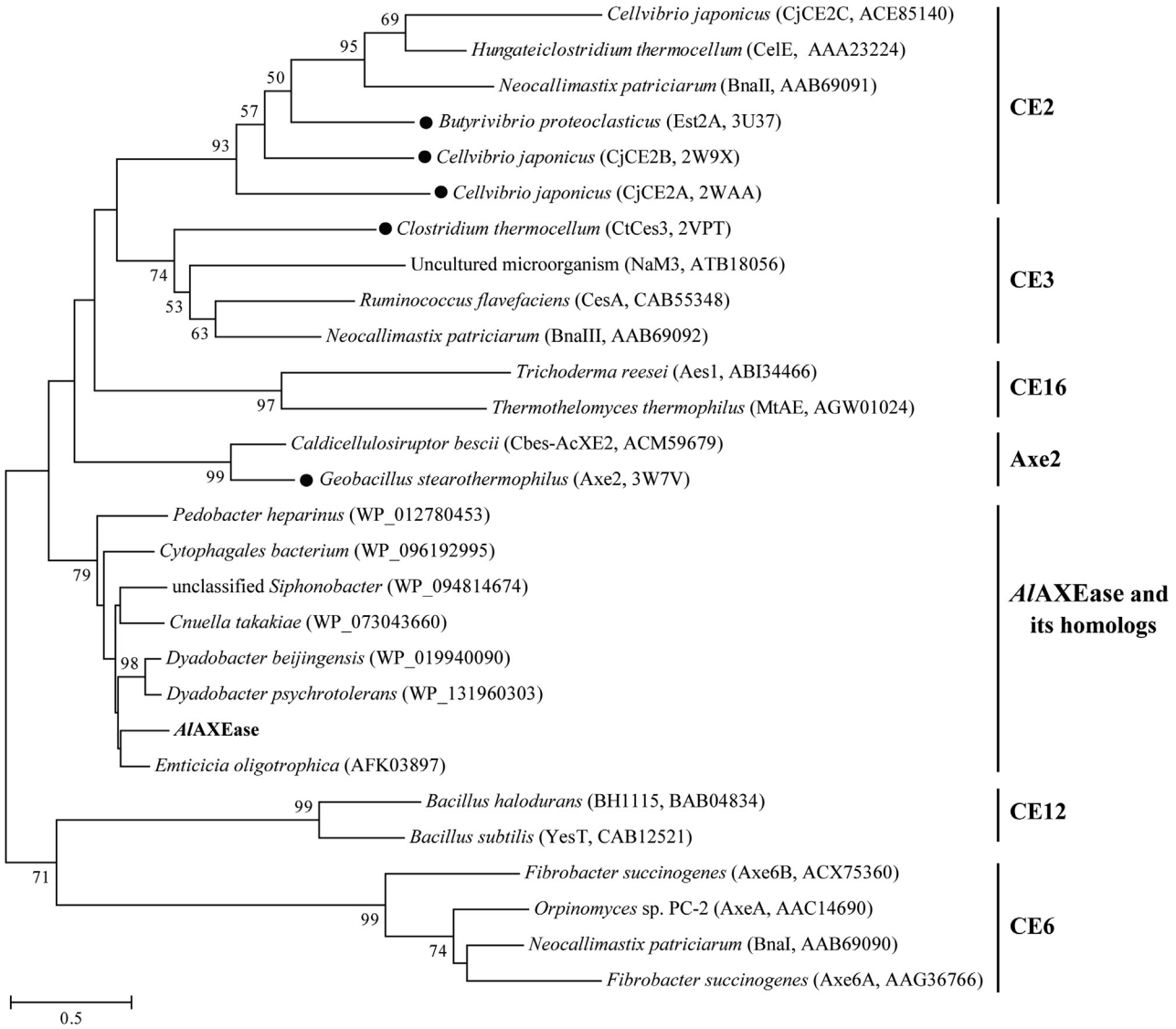

Figure 1. Phylogenetic analysis of *Al*AXEase and reported SGNH-type AcXEs. The tree was built by the neighbor-joining method with a JTT matrix–based mode using 112 amino acid positions. Bootstrap analysis of 1000 replicates is executed, and values above 50% are shown. AcXEs with structures are indicated by *black circles*. AcXEs, acetyl xylan esterases; *Al*AXEase, a cold-adapted AcXE from Arctic marine bacterium *Arcticibacterium luteifluviistationis* SM1504^{T}.

activity, whereas the other metal ions had no or weak inhibitory effect on *Al*AXEase activity (Table 2). *Al*AXEase activity was not influenced by the metal chelator EDTA but severely inhibited by 10 mM PMSF (Table 2), suggesting that *Al*AXEase is a serine hydrolase.

To reveal the natural substrates of *Al*AXEase, we also measured the activity of *Al*AXEase against different kinds of acetylated carbohydrates (Table 1). Similar to the acetyl xylan esterase Axe2 from *G. stearothermophilus* (Table S1), *Al*AXEase could deacetylate many acetylated monosaccharides and disaccharides including galactose, glucose, xylose in furanose and pyranose configurations, sucrose, and xylobioside, as well as partially acetylated xylan, with the highest activity toward acetylated glucose and xylopyranose (Table 1), indicating that *Al*AXEase is a CE. *Al*AXEase hardly degraded *N*-acetyl-D-glucosamine (Table 1), suggesting its high specificity for the O-acetyl groups rather than the N-acetyl groups of acetylated carbohydrates. Further kinetic analysis revealed that, among the acetylated monosaccharides, acetylated xylopyranose is the optimal substrate of *Al*AXEase, to which *Al*AXEase showed the highest substrate affinity and the highest catalytic efficiency (k_{cat}/K_m) (Fig. 3*F* and Table S2). Moreover, *Al*AXEase could hydrolyze both acetylated xylobioside and acetyl xylan (Table 1). All these data indicate that *Al*AXEase is an acetyl xylan esterase.

Analysis of the overall structure and the active site of Al*AXEase*

To reveal the underlying cold adaption mechanism of *Al*AXEase, we solved the crystal structure of WT *Al*AXEase by the molecular replacement method using selenomethionine (SeMet)-*Al*AXEase structure as the starting model because of the low sequence identities (lower than 24%) shared by *Al*AXEase and proteins with available structures in the Protein

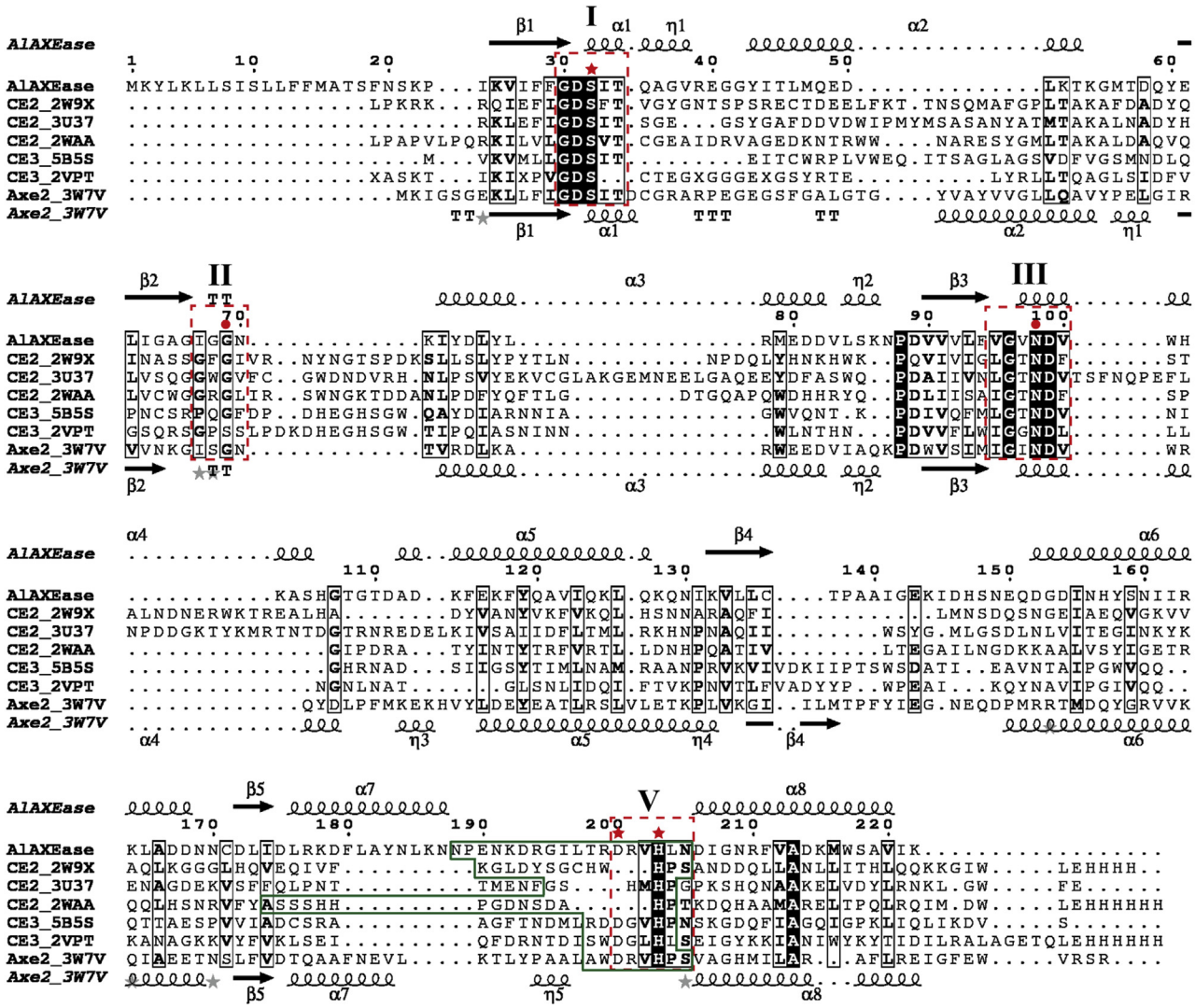

Figure 2. Multiple sequence alignment of *Al*AXEase and reported SGNH-type AcXEs with structures. Using ESPript, secondary structures of *Al*AXEase are shown above alignment and secondary structures of Axe2 (PDB code 3W7V) under alignment. Helices are indicated by *squiggles*, β strands by *arrows*, turns by *TT letters*, and 3_{10}-helices by *η letters*. Identical amino acid residues are shown in *white* on a *black shadow*, and similar residues are in *bold black*. *Stars* represent residues belonging to the catalytic triad, and *circles* represent oxyanion hole residues. The four conserved sequence blocks in SGNH hydrolases are *boxed* by *red dashed lines*. The catalytic loop in *Al*AXEase and the corresponding loops in other SGNH-type AcXEs are *boxed* by *green solid lines*. AcXEs, acetyl xylan esterases; *Al*AXEase, a cold-adapted AcXE from Arctic marine bacterium *Arcticibacterium luteifluviistationis* SM1504[T]; PDB, Protein Data Bank.

Data Bank (PDB) database. The crystal of *Al*AXEase belongs to the $P12_11$ space group, and the structure of *Al*AXEase was solved at 2.50 Å resolution. The statistics for refinement are summarized in Table 3. Structural data show that each asymmetric unit contains four *Al*AXEase molecules (Fig. 4*A*). Gel filtration analysis showed that *Al*AXEase tends to form large oligomers in solutions (Fig. 4*B*), and dynamic light scattering (DLS) analysis indicated that *Al*AXEase forms stable tetramers in solutions (Fig. 4*C*).

The overall structure of *Al*AXEase monomer is similar to those of other SGNH-type AcXEs (Fig. 4*D*), most closely resembling the structures of an uncharacterized GDSL protein (PDB code 3RJT) from *Alicyclobacillus acidocaldarius* and Axe2 (PDB code 3W7V) from *G. stearothermophilus* (15), with the RMSD of 1.34 Å (150 monomer Cα atoms) and 2.63 Å (147 monomer Cα atoms), respectively. Monomeric *Al*AXEase shows a typical SGNH hydrolase fold, consisting of a central four-stranded parallel sheet flanked by two layers of helices (Fig. 4*E*). Similar to most AcXEs (1, 14, 15), *Al*AXEase has a catalytic triad formed by residues Ser32, Asp200, and His203, which are all located on the protein surface (Fig. 4*F*). Ser32 is situated on the terminus of α1, while Asp200 and His203 are located in a long surface loop between α7 and α8 (Fig. 4*E*). Mutation of these residues to Ala led to extremely low or no enzymatic activity (Table 4), demonstrating their key roles in the catalysis. The oxyanion hole is composed of two solvent-exposed residues, Gly69 and Asn98 (Fig. 4*F*). Both mutations G69A and N98A had a small impact on the K_m, but significantly decreased the k_{cat} of *Al*AXEase (Table 4), consistent with that the oxyanion hole residues are involved in stabilizing the tetrahedral intermediates in the reaction process through their main-chain nitrogen atoms (27). The catalytic residues

Table 1
The substrate specificity of *Al*AXEase

Substrate	Specific activity (U/mg)
p-Nitrophenyl acetate	9.10 ± 0.09
p-Nitrophenyl butyrate	–[a]
p-Nitrophenyl caproate	–[a]
p-Nitrophenyl caprylate	–[a]
1-Napthyl acetate	2.21 ± 0.18
Phenyl acetate	2.23 ± 0.44
Isopropenyl acetate	–[a]
Menthyl acetate	0.40 ± 0.09
Florfenicol	0.07 ± 0.01
Ethyl 2-chlorobenzoate	0.10 ± 0.01
Ethyl 4-chloro-3-hydroxybutanoate	0.10 ± 0.01
β-D-galactose pentaacetate	3.63 ± 0.01
β-D-glucose pentaacetate	3.89 ± 0.06
Sucrose octaacetate	3.61 ± 0.34
1,2,3,5-Tetra-O-acetyl-D-xylofuranose	3.02 ± 0.21
1,2,3,4-Tetra-O-acetyl-D-xylopyranose	3.88 ± 0.14
Benzyl β-D-xylobioside pentaacetate	0.38 ± 0.03
Xylan (partially acetylated)	0.29 ± 0.03
N-acetyl-D-glucosamine	–[a]

[a] Undetectable.

Table 2
Effects of metal ions and potential inhibitors on *Al*AXEase activity

	Relative/residual activity (%)	
Compound	1 mM	10 mM
K^+	104.1 ± 0.7	111.4 ± 1.85
Li^+	105.9 ± 0.9	61.0 ± 2.9
Ba^{2+}	112.1 ± 2.4	103.1 ± 2.2
Ca^{2+}	110.1 ± 1.5	136.0 ± 1.9
Co^{2+}	102.1 ± 0.7	70.8 ± 1.7
Cu^{2+}	84.7 ± 0.3	4.85 ± 0.3
Fe^{2+}	125.3 ± 3.4	5.3 ± 4.5
Mg^{2+}	110.0 ± 2.0	118.2 ± 1.1
Mn^{2+}	107.1 ± 0.9	127.1 ± 1.4
Ni^{2+}	105.9 ± 0.9	61.0 ± 2.9
Sr^{2+}	108.4 ± 1.1	111.5 ± 1.7
Zn^{2+}	105.1 ± 1.2	59.3 ± 0.5
Fe^{3+}	111.4 ± 6.0	–[a]
EDTA	104.4 ± 1.7	101.0 ± 1.5
PMSF	77.5 ± 1.1	38.4 ± 1.1

[a] Undetectable.

and the oxyanion hole residues together with their adjacent residues form a shallow substrate-binding pocket of *Al*AXEase (Fig. 4*F*).

In the *Al*AXEase tetramer, the interface between chains B and C is the largest, followed by the interface between chains C and D, and the remaining interfaces involving chain A are the least (Fig. 5*A*). The dimerization interface between chains B and C is mainly stabilized by hydrogen bonds and salt bridges involving eight residues Lys (71, 114), Gly (69, 107, 109), Asp (74, 111), and Thr108 from the interactive monomers (Fig. 5*B*), and the interface between chains C and D mainly by four hydrophilic residues Asp146, His147, Asn156, and Asn160 (Fig. 5*C*).

Structural basis for the high thermostability of Al*AXEase*

Among all the characterized proteins, the sequence and topological structure of *Al*AXEase are most closely related to

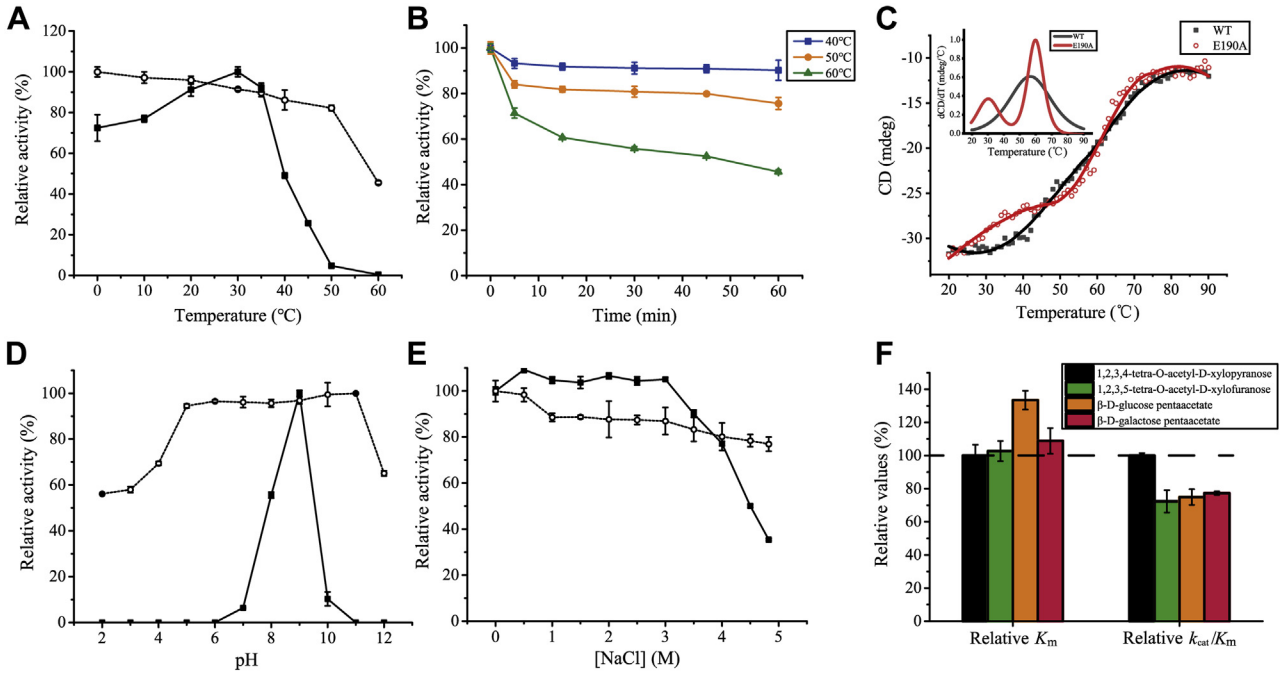

Figure 3. Biochemical characterization of *Al*AXEase. *A*, the effect of the temperature on the activity (*solid line*) and stability (*dashed line*) of *Al*AXEase. *B*, the effect of the temperature on the stability of *Al*AXEase. The enzyme was incubated at 40 °C, 50 °C, and 60 °C for different time intervals, and the residual activity was measured at pH 8.0 and 30 °C. *C*, thermal unfolding of *Al*AXEase and its mutant monitored by CD. The CD was monitored at 222 nm. The temperature was monitored using an internal sensor with a gradient of 1.0 °C per min. The inset shows the first derivative of the CD signal *versus* temperature. The data shown are representative of results of triplicate experiments. *D*, the effect of pH on the activity (*solid line*) and stability (*dashed line*) of *Al*AXEase. For stability, the enzyme was incubated in buffers ranging from pH 2.0 to 12.0 at 0 °C for 1 h, and the residual activity was measured at pH 8.0 and 30 °C. *E*, the effect of NaCl on the activity (*solid line*) and stability (*dashed line*) of *Al*AXEase. For stability, the enzyme was incubated at 0 °C for 1 h in buffers containing NaCl ranging from 0 to 4.8 M, and the residual activity was measured at pH 8.0 and 30 °C. *F*, kinetic parameters of *Al*AXEase against different acetylated monosaccharides. Enzyme kinetic assays of *Al*AXEase were carried out at pH 9.0 (20 mM Hepes) using 1,2,3,4-tetra-O-acetyl-D-xylopyranose, 1,2,3,5-tetra-O-acetyl-D-xylofuranose, β-D-glucose pentaacetate, and β-D-galactose pentaacetate at concentrations from 0.5 to 20 mM, respectively. The K_m and k_{cat}/K_m values of *Al*AXEase against 1,2,3,4-tetra-O-acetyl-D-xylopyranose are considered to be 100%. In panels *A*, *B*, *D*, *E*, and *F*, the graphs show data from triplicate experiments (mean ± SD). *Al*AXEase, a cold-adapted AcXE from Arctic marine bacterium *Arcticibacterium luteifluviistationis* SM1504^T.

Table 3
Data collection and refinement statistics of WT *Al*AXEase and SeMet-*Al*AXEase

Parameters	*Al*AXEase	SeMet-*Al*AXEase
Data collection		
Space group	$P12_11$	$P12_11$
Unit cell dimensions		
a, b, c (Å)	76.87, 80.61, 82.06	72.22, 79.04, 81.80
α, β, γ (°)	90, 103.132, 90	90, 104.28, 90
Wavelength (Å)	0.9791	0.9791
Resolution range (Å)	50.00–2.50 (2.54–2.50)[a]	50.00–2.30 (2.34–2.30)
Redundancy	3.4 (3.5)	3.0 (2.3)
Completeness (%)	98.8	91.6
R_{merge}[b]	0.137 (0.306)	0.153 (0.437)
I/sigma	8.25 (2.67)	8.94 (1.27)
Refinement statistics		
Resolution range (Å)	42.07–2.51 (2.60–2.51)	
R_{work} (%)	17.92 (20.02)	
R_{free} (%)	23.54 (26.95)	
B-factor (Å^2)		
Macromolecules	28.09	
Solvent	29.64	
RMSD from ideal geometry		
Bond lengths (Å)	0.01	
Bond angles (°)	1.02	
Ramachandran plot (%)		
Favored (%)	93.91	
Allowed (%)	6.09	

[a] Numbers in parentheses refer to data in the highest resolution shell.
[b] $R_{merge} = \Sigma_{hkl}\Sigma_i|I(hkl)_i - \langle I(hkl)\rangle|/\Sigma_{hkl}\Sigma_i \langle I(hkl)_i\rangle$.

those of Axe2 albeit with a low similarity of 24% (Figs. 1 and 4). Axe2 is a mesophilic enzyme with the highest activity between 50 °C and 60 °C and a T_m value of 72 °C (4). The most common determinants for increased thermostability of hyperthermophilic proteins are more noncovalent stabilizing interactions (21, 28, 29). At the monomer level, *Al*AXEase has

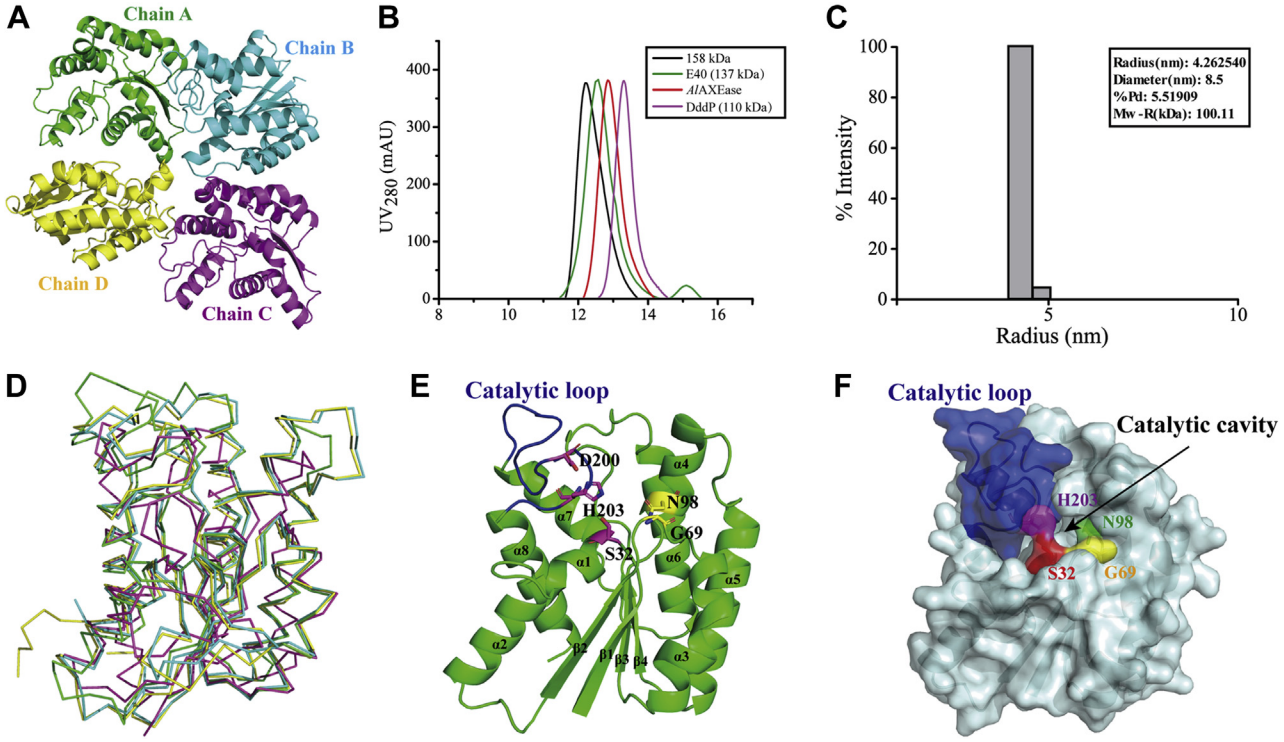

Figure 4. Overall structural analysis of *Al*AXEase. *A*, overall structure of tetrameric *Al*AXEase in one asymmetric unit. *B*, gel filtration analysis of *Al*AXEase. Aldolase (158 kDa), protein E40 (137 kDa) (48), and protein DddP (110 kDa) (49) were used as protein size markers. The theoretical molecular weight of monomeric *Al*AXEase without signal peptide is 23.5 kDa. *C*, DLS analysis of *Al*AXEase. *D*, superimposition of *Al*AXEase and other SGNH-type enzymes. *Al*AXEase is colored in *green*, the uncharacterized GDSL protein (PDB code 3RJT) from *Alicyclobacillus acidocaldarius* in *cyan*, CtCes3 (PDB code 2VPT) in *magenta*, and Axe2 (PDB code 3W7V) in *yellow*. *E*, overall structure of monomeric *Al*AXEase. The monomer has four β-sheets and eight α-helices. The catalytic triad residues (Ser32, Asp200, and His203) and the oxyanion hole residues (Gly69 and Asn98) are shown as *sticks*. The catalytic loop is colored in *blue*. *F*, surface view of monomeric *Al*AXEase. Active site residues Ser32, Gly69, Asn98, and His203 are colored in *red*, *yellow*, *green*, and *magenta*, respectively, and the catalytic loop in *blue*. *Al*AXEase, a cold-adapted AcXE from Arctic marine bacterium *Arcticibacterium luteifluviistationis* SM1504^T; DLS, dynamic light scattering.

Table 4
Kinetic parameters of *Al*AXEase and its mutants against 1,2,3,4-tetra-O-acetyl-D-xylopyranose

Enzyme	Temperature (°C)	V_{max} (μM/min/mg)	K_m (mM)	k_{cat} (s^{-1})	k_{cat}/K_m (mM^{-1} s^{-1})
WT	10	5.2 ± 0.17	3.4 ± 0.08	2.0 ± 0.07	0.60 (83%)
WT	20	7.2 ± 0.01	4.5 ± 0.35	2.8 ± 0.01	0.63 (88%)
WT	30	9.2 ± 0.46	5.0 ± 0.33	3.6 ± 0.18	0.72 (100%)
WT	40	4.6 ± 0.67	5.6 ± 0.57	1.8 ± 0.26	0.33 (46%)
WT	50	1.0 ± 0.06	6.1 ± 0.16	0.41 ± 0.02	0.07 (10%)
S32A	30	–[a]	–[a]	–[a]	–[a]
G69A	30	3.1 ± 0.04	5.3 ± 0.30	1.2 ± 0.01	0.23 (31%)
N98A	30	0.05 ± 0.01	6.0 ± 0.36	0.02 ± 0.01	0.01 (1.4%)
D200A	30	0.05 ± 0.02	5.0 ± 0.16	0.02 ± 0.01	0.01 (1.4%)
H203A	30	–[a]	–[a]	–[a]	–[a]
E190A	10	4.4 ± 0.37	3.6 ± 0.25	1.7 ± 0.14	0.45 (63%)
E190A	20	5.7 ± 0.95	5.6 ± 0.21	2.2 ± 0.37	0.49 (68%)
E190A	30	2.0 ± 0.06	6.0 ± 0.16	0.77 ± 0.02	0.13 (18%)
E190A	40	0.48 ± 0.10	6.7 ± 0.13	0.19 ± 0.04	0.03 (4.2%)
E190A	50	–[a]	–[a]	–[a]	–[a]

[a] Undetectable.

similar numbers of hydrogen bonds and ionic interactions as Axe2 (Table 5), suggesting that *Al*AXEase has a high overall stability, thus leading to the high thermostability of *Al*AXEase. From psychrophiles to mesophiles to thermophiles, a clear trend can be observed that shows an increase in the number of ionic attractions on the protein surface (23, 30). Compared with Axe2, *Al*AXEase has a more positively charged interface near its active site (Fig. 6*A*), fewer stabilizing prolines, and more thermally labile residues asparagine and lysine on its surface (Table 5 and Fig. 6, *B* and *C*), which may result in the lower thermostability of *Al*AXEase than Axe2.

In addition, oligomerization also contributes to the thermal stability of proteins (31, 32). Axe2 forms a 'doughnut-shaped' homo-octamer with two staggered tetrameric rings both in the crystal and in solution, and the oligomerization of Axe2 is mainly stabilized by a cluster of hydrogen bonds and π-stacking interactions involving residues near the active sites of all eight monomers (15). Similar to Axe2, *Al*AXEase also forms large oligomers. *Al*AXEase forms tetramers both in the crystal and solution (Fig. 4), which may play a role in maintaining the structural stability and thermostability of *Al*AXEase. Different from Axe2 octamers, *Al*AXEase tetramers are mainly maintained by residues far away from their active sites (Fig. 5). Moreover, the smaller oligomerization interfaces of *Al*AXEase than those of Axe2 suggest that *Al*AXEase tetramers are less compact than Axe2 octamers, which may also contribute to the lower thermostability of *Al*AXEase.

*Al*AXEase has a long and flexible catalytic loop around its active site

At the monomer level, the largest structural difference between *Al*AXEase and Axe2 is that the loop containing the

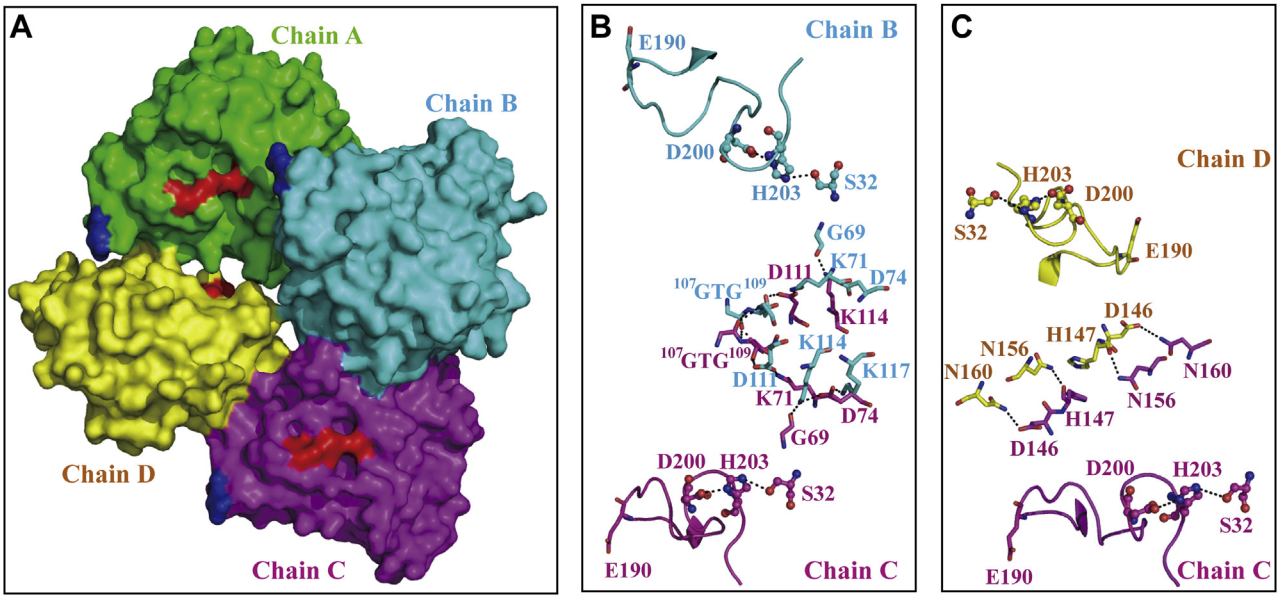

Figure 5. Oligomerization of *Al*AXEase. *A*, surface view of tetrameric *Al*AXEase. The four chains of *Al*AXEase are shown in different colors, and the catalytic triad and the residue Glu190 in the catalytic loop of each chain are highlighted in *red* and *blue*, respectively. *B*, the hydrogen-bond network between chains B and C. Residues in chain B are shown in *cyan*, and residues in chain C in *magenta*. For both chains, catalytic triad residues are shown in *ball-and-stick* representation. *C*, the hydrogen-bond network between chains C and D. Residues in chain C are shown in *magenta* and residues in chain D in *yellow*. For both chains, catalytic triad residues are shown in *ball-and-stick* representation. *Al*AXEase, a cold-adapted AcXE from Arctic marine bacterium *Arcticibacterium luteifluviistationis* SM1504[T].

Table 5
Structure and sequence comparison of *Al*AXEase and Axe2

Sequence/structural information	*Al*AXEase[a]	Axe2[b]
T_m (°C)	56	72
T_{opt} (°C)	30	50–60
Recombinant protein sequence length	208	219
Hydrophobic residues[c] (%)	38.5	45.7
Polar residues[d] (%)	31.7	27.9
Charged residues[e] (%)	29.8	26.5
Net charges (Arg + Lys - Asp - Glu)	−3	−3
No. of Gly/Met/Pro	16/5/4	19/7/9
No. of Asn/Gln	16/8	6/7
Arg/(Arg + Lys)	0.296	0.577
Sequence identity to *Al*AXEase	100%	24%
PDB entry	This study	3W7V
Resolution (Å)	2.50	1.85
No. of residues per monomer in the crystal structure	199 ± 1	219 ± 0
RMSD (Å) (no. of residues)		2.69 ± 0.09 (148 ± 2)
No. of hydrogen bonds per residue in monomer	2.374 ± 0.04	2.297 ± 0.04
No. of side-chain to side-chain hydrogen bonds per residue	0.398 ± 0.04	0.416 ± 0.05
No. of side-chain to main-chain hydrogen bonds per residue	0.550 ± 0.02	0.506 ± 0.03
No. of main-chain to main-chain hydrogen bonds per residue	1.426 ± 0.02	1.374 ± 0.03
No. of ion pairs per monomer at 4 Å	12 ± 1.6	14 ± 2.8
No. of ion pairs per monomer at 6 Å	22.5 ± 0.6	26 ± 2.8
No. of ion pairs per residue (4 Å)	0.060 ± 0.01	0.064 ± 0.01

[a] No. of hydrogen bonds and ion pairs were calculated based on the four chains in the crystal structure of WT *Al*AXEase.
[b] No. of hydrogen bonds and ion pairs were calculated based on the two chains in the crystal structure of Axe2.
[c] Hydrophobic residues A, V, L, I, W, F, P, and M.
[d] Polar residues G, S, T, Y, N, Q, and C.
[e] Charged residues R, K, H, D, and E.

catalytic residues Asp200 and His203 (18 residues in length) in *Al*AXEase is much longer than the corresponding one in Axe2 (8 residues in length) (Fig. 7*A*). The catalytic loop of *Al*AXEase is also the longest one among all the characterized AcXEs with solved structures (Fig. 2). Based on the B factor analysis, the flexible regions in *Al*AXEase and Axe2 are similar, except that the active site of *Al*AXEase is more flexible, especially the long catalytic loop (Fig. 6*C*). In *Al*AXEase, the catalytic loop is mainly stabilized by forming hydrogen bonds with two residues (Glu143 and Asp146) in the loop between β4 and α6 and hydrophobic interactions involving four residues (Ile196, Leu197, Val202, and Leu204) in the catalytic loop and eight hydrophobic residues in the other regions of *Al*AXEase (Fig. 7, *B* and *D*). For Axe2, similar hydrogen bonds and hydrophobic interactions are found to stabilize its short catalytic loop (Fig. 7, *C* and *E*). However, *Al*AXEase has less hydrophobic interactions (a 12-member cluster) around the catalytic loop than Axe2 (a 16-member cluster) (Fig. 7*F*). Moreover, no interaction is present to maintain the structure of the region ^{192}KDRG^{195} in the catalytic loop of *Al*AXEase (Fig. 7, *B* and *D*), and this region and its upstream residues are rich in destabilizing asparagine and lysine residues (Fig. 6*B*). In addition, the catalytic loop in Axe2 also forms intermolecular hydrogen bonds between interactive monomers (15), which, however, are absent from *Al*AXEase. All these differences make the catalytic loop of *Al*AXEase more flexible than that in Axe2, which would improve the flexibility of the catalytic center and lead to the high activity of *Al*AXEase at low temperatures. When the catalytic loop in *Al*AXEase was shortened (mutants △2 and △3 in Fig. 8*A*) or substituted by the short catalytic loop of Axe2 (mutants L1 and L2 in Fig. 8*A*), all the mutants were inactive (Fig. 8*A*), indicating that the length and flexibility of the catalytic loop is important for maintaining the catalytic activity of *Al*AXEase.

The catalytic loop contributes to the cold-adapted characteristics of AlAXEase by modulating the distance between the catalytic residues Ser32 and His203

To further investigate the role of the catalytic loop in the cold adaptation of *Al*AXEase, site-directed mutagenesis on the residue Glu190 in the catalytic loop with the highest B factor was performed. Compared with WT *Al*AXEase, mutant E190A had a lower optimum temperature (T_{opt}) of 20 °C (Figs. 3*A* and 8*B*). At 10 °C, mutant E190A retained 92% of its maximal catalytic efficiency (k_{cat}/K_m), higher than that of the WT (83%) (Table 4), suggesting that mutant E190A is more active than the WT at low temperatures. Mutant E190A also had a lower thermostability, quite unstable at temperatures above 20 °C (Fig. 8, *B* and *C*). These data suggest that mutant E190A is more cold-adapted than WT *Al*AXEase.

Then, structural analyses and MD simulations of WT *Al*AXEase and its mutant E190A at different temperatures were carried out to further probe the molecular mechanism for the cold adaptation of *Al*AXEase (Figs. 9 and 10 and Fig. S3). At all simulated temperatures, no significant differences were observed in the RMSD values of the backbone atoms of both enzymes (Fig. 10*A*), suggesting that the introduction of the E190A mutation in the catalytic loop has little impact on the overall structures of *Al*AXEase monomers under different temperatures. However, the fluorescence peak position of *Al*AXEase began to change with a blue shift at 60 °C, and that of mutant E190A at 20 °C (Fig. 9*A*), indicating that the tertiary structure of the mutant is less rigid and less stable than that of the WT against high temperatures. Moreover, different from the WT (with a T_m value of 56 °C), mutant E190A presented two thermal transitions (Fig. 3*C*), one at ∼30 °C and the other at ∼60 °C, suggesting that some regions of the enzyme unfold first at a low temperature, followed by the unfolding of the

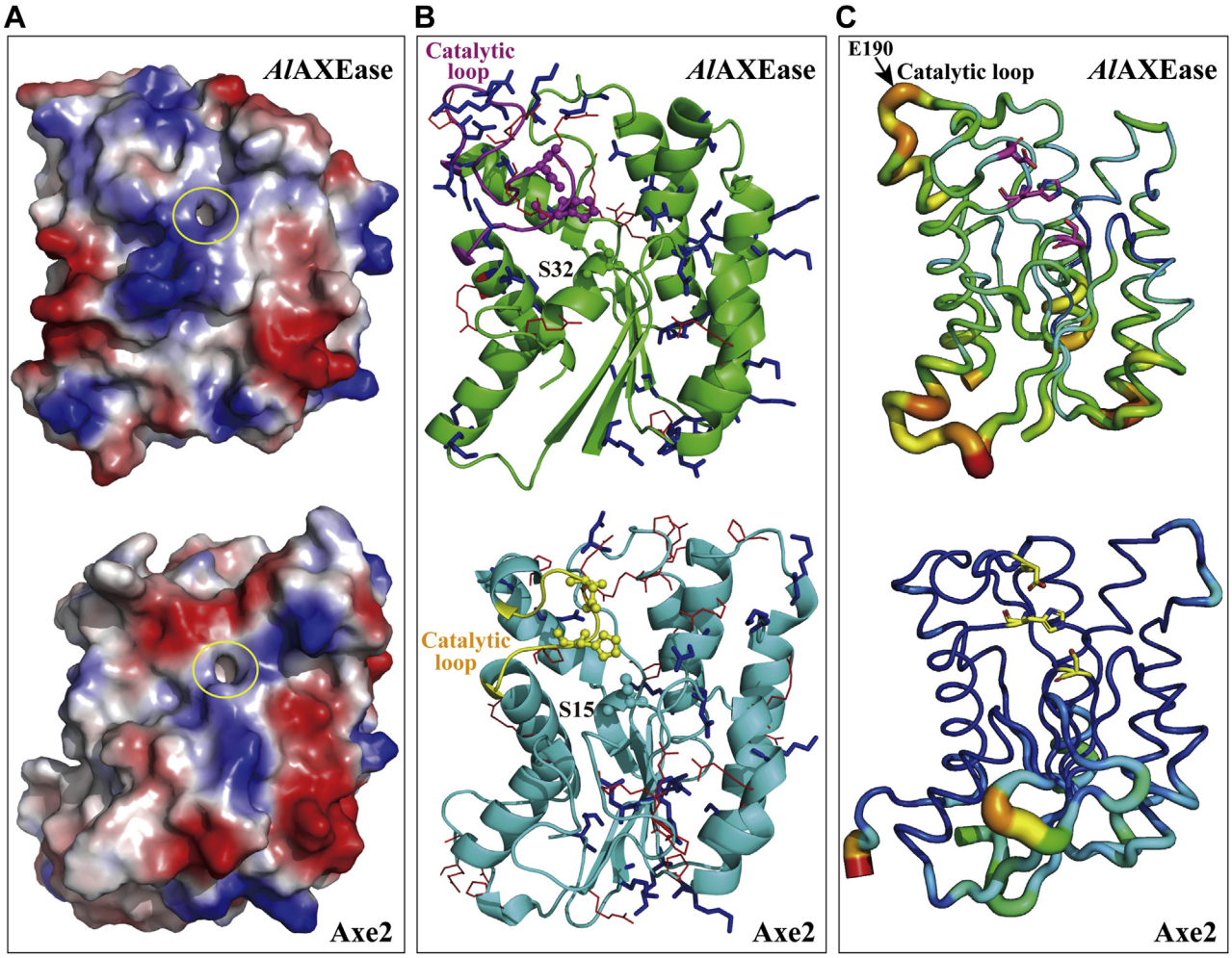

Figure 6. Comparative structural analysis of cold-adapted *Al*AXEase and mesophilic Axe2. *A*, electrostatic surfaces of *Al*AXEase and Axe2. The positively charged regions are shown in *blue* and the negatively charged regions in *red*. The catalytic cavities of *Al*AXEase and Axe2 are marked with *yellow circles*. *B*, *cartoon* view of *Al*AXEase and Axe2. For both *Al*AXEase and Axe2, stabilizing residues Arg and Pro are shown as *red lines*, destabilizing residues Asn and Lys as *blue sticks*, and catalytic triad residues in *ball-and-stick* representation. Catalytic loop in *Al*AXEase is colored in *magenta*, and the counterpart in Axe2 in *yellow*. *C*, B factor analysis of *Al*AXEase and Axe2. The thicker coils show higher flexibility than other parts of the protein. The catalytic triad residues of *Al*AXEase and Axe2 are shown as *sticks*. *Al*AXEase, a cold-adapted AcXE from Arctic marine bacterium *Arcticibacterium luteifluviistationis* SM1504^T.

remaining regions at relatively high temperature. These data suggest that the introduced mutation E190A may cause an increased flexibility in local rather than overall structure of *Al*AXEase to enhance its cold adaptation.

Root mean square fluctuation values often reflect the fluctuation of individual residues during the MD simulation process (33). As shown in Figure 10*B*, both *Al*AXEase and its mutant contain three major unstable regions, including (1) the loop between β2 and α3 and the initial proportion of α3 (residues 67–76), (2) the latter part of α4 and the loop between α4 and α5 (residues 103–111), and (3) the region near the active site involving the catalytic loop. The latter part of the loop between β4 and α6 (residues 143–152) is also unstable in *Al*AXEase but stable in the mutant. Except for the unstable regions near the active site, all other unstable regions are located in the oligomerization interfaces of *Al*AXEase (Fig. 5), suggesting that heat treatment may influence the oligomerization of protein. Notably, at 45 °C, *Al*AXEase lost most of the enzymatic activity (Fig. 3*A*) but still retained tetramers (Fig. 9*B*), demonstrating that the cold-adapted characteristics of *Al*AXEase come from the flexibility of its monomeric rather than oligomeric structure. Different from the WT, a part of the tetramers of mutant E190A were depolymerized to monomers at its T_{opt} of 20 °C (Fig. 9*B*), suggesting that the introduced mutation E190A makes *Al*AXEase tetramers tend to depolymerize to decrease its thermostability.

MD simulations also showed that the regions around the active sites of both *Al*AXEase and mutant E190A become flexible at a high temperature (Fig. 10*B*). Compared with the small unstable part of the catalytic loop (residues 201 and 202) in *Al*AXEase, mutant E190A possessed a larger unstable region around the active site including the α7 and the following long catalytic loop (residues 180–194, 201, and 202) (Fig. 10*B*). It has been found that high flexibility, particularly around the active site, is usually associated with low substrate affinity in cold-adapted enzymes (21, 24). Similarly, compared with Axe2, *Al*AXEase and mutant E190A showed increased K_m values, and the K_m values of mutant E190A were higher than those of *Al*AXEase (Table 4 and Table S3), further indicating a flexible active site in *Al*AXEase and a more flexible active site in the

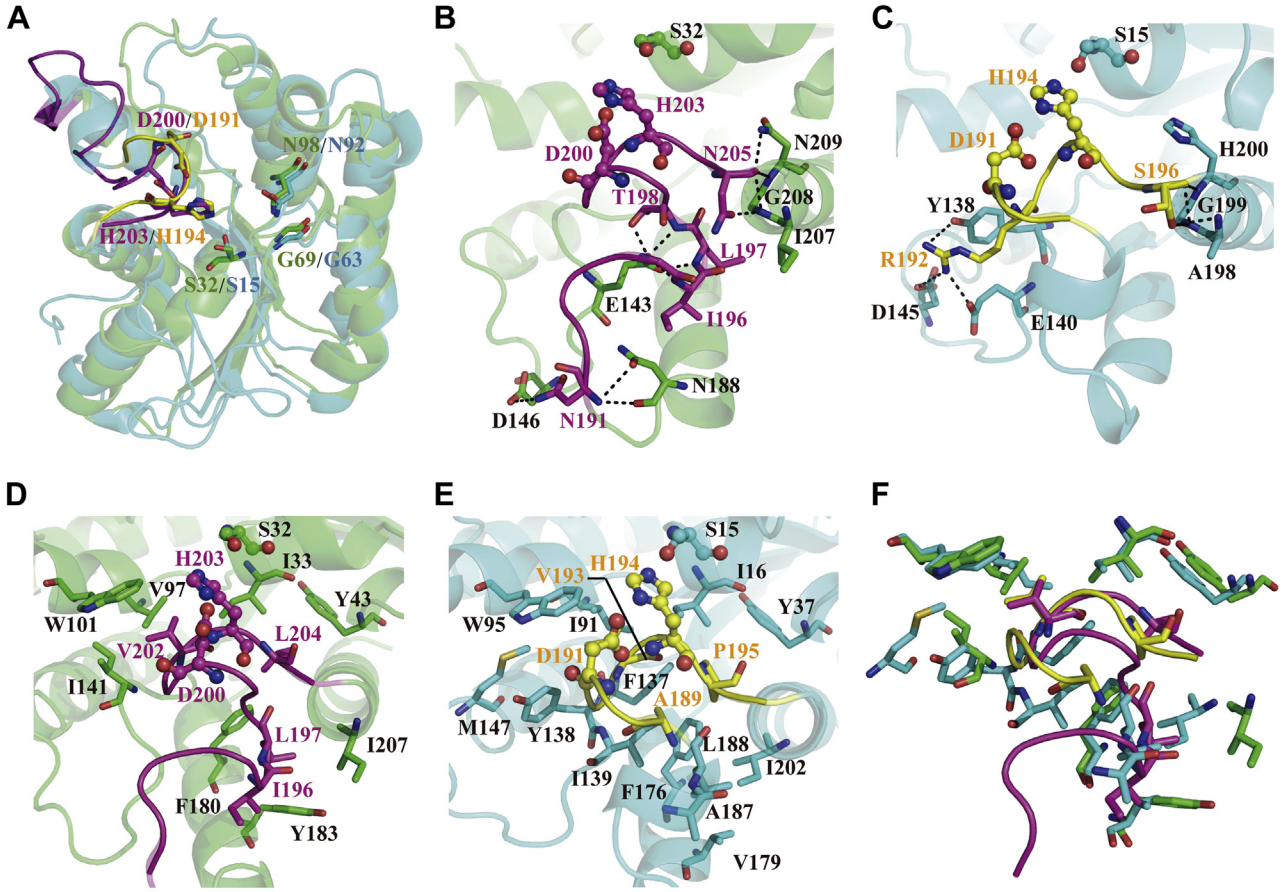

Figure 7. Analysis of the interactions between the catalytic loop and other regions in *Al*AXEase and Axe2. *A*, the superimposition of *Al*AXEase (*green*) and Axe2 (*cyan*). Catalytic loop in *Al*AXEase is colored in *magenta*, and the counterpart in Axe2 in *yellow*. For both *Al*AXEase and Axe2, the catalytic triad residues and the oxyanion hole residues are shown as *sticks*. *B*, the hydrogen-bond network between the catalytic loop (*magenta*) and other regions (*green*) in *Al*AXEase. Key residues involved in these interactions are shown as *sticks*. *C*, the hydrogen-bond network between the catalytic loop (*yellow*) and other regions (*cyan*) in Axe2. Key residues involved in these interactions are shown as *sticks*. *D*, the hydrophobic interactions between the catalytic loop (*magenta*) and other regions (*green*) in *Al*AXEase. Key hydrophobic residues are shown as *sticks*. *E*, the hydrophobic interactions between the catalytic loop (*yellow*) and other regions (*cyan*) in Axe2. Key hydrophobic residues are shown as *sticks*. In panels *B–E*, the catalytic triads are in *ball-and-stick* representation. *F*, the superimposition of hydrophobic residues in *Al*AXEase and Axe2 involved in the hydrophobic interactions between the catalytic loop (*magenta* for *Al*AXEase and *yellow* for Axe2) and other regions (*green* for *Al*AXEase and *cyan* for Axe2). *Al*AXEase, a cold-adapted AcXE from Arctic marine bacterium *Arcticibacterium luteifluviistationis* SM1504^{T}.

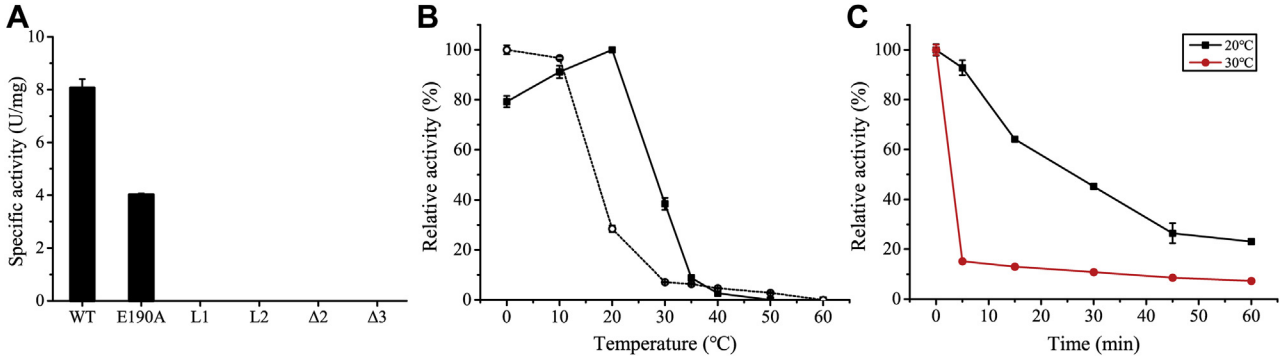

Figure 8. Analyses of the thermodependence of activity and thermostability of mutant E190A. *A*, enzymatic activities of the mutants of *Al*AXEase. Mutant L1 with mutation to replace residues ^{185}LKNNPENKDRGILTR^{199} in the catalytic loop of *Al*AXEase with ^{181}KTLYPAALAW^{190} of Axe2, mutant L2 with mutation to replace residues ^{185}LKNNPENKDRGI^{196} of *Al*AXEase with ^{181}KTLYPAA^{187} of Axe2, mutant Δ2 with mutation to delete residues Asn188 and Pro189 of *Al*AXEase, and mutant Δ3 with mutation to delete residues Asn188, Pro189, and Glu190 of *Al*AXEase. The activities of WT *Al*AXEase and mutant E190A were measured under their respective optimum temperatures. For all other mutants, no enzymatic activity was detected at temperatures ranging from 0 to 60 °C. *B*, the effect of temperature on the activity (*solid line*) and stability (*dashed line*) of mutant E190A. For stability, the enzyme was incubated from 0 to 60 °C for 1 h, and the residual activity was measured under optimal conditions. *C*, the effect of the temperature on the stability of mutant E190A. The enzyme was incubated at 20 °C and 30 °C for different time intervals, and the residual activity was measured under optimal conditions. In panels *A–C*, the graphs show data from triplicate experiments (mean ± SD). *Al*AXEase, a cold-adapted AcXE from Arctic marine bacterium *Arcticibacterium luteifluviistationis* SM1504^{T}.

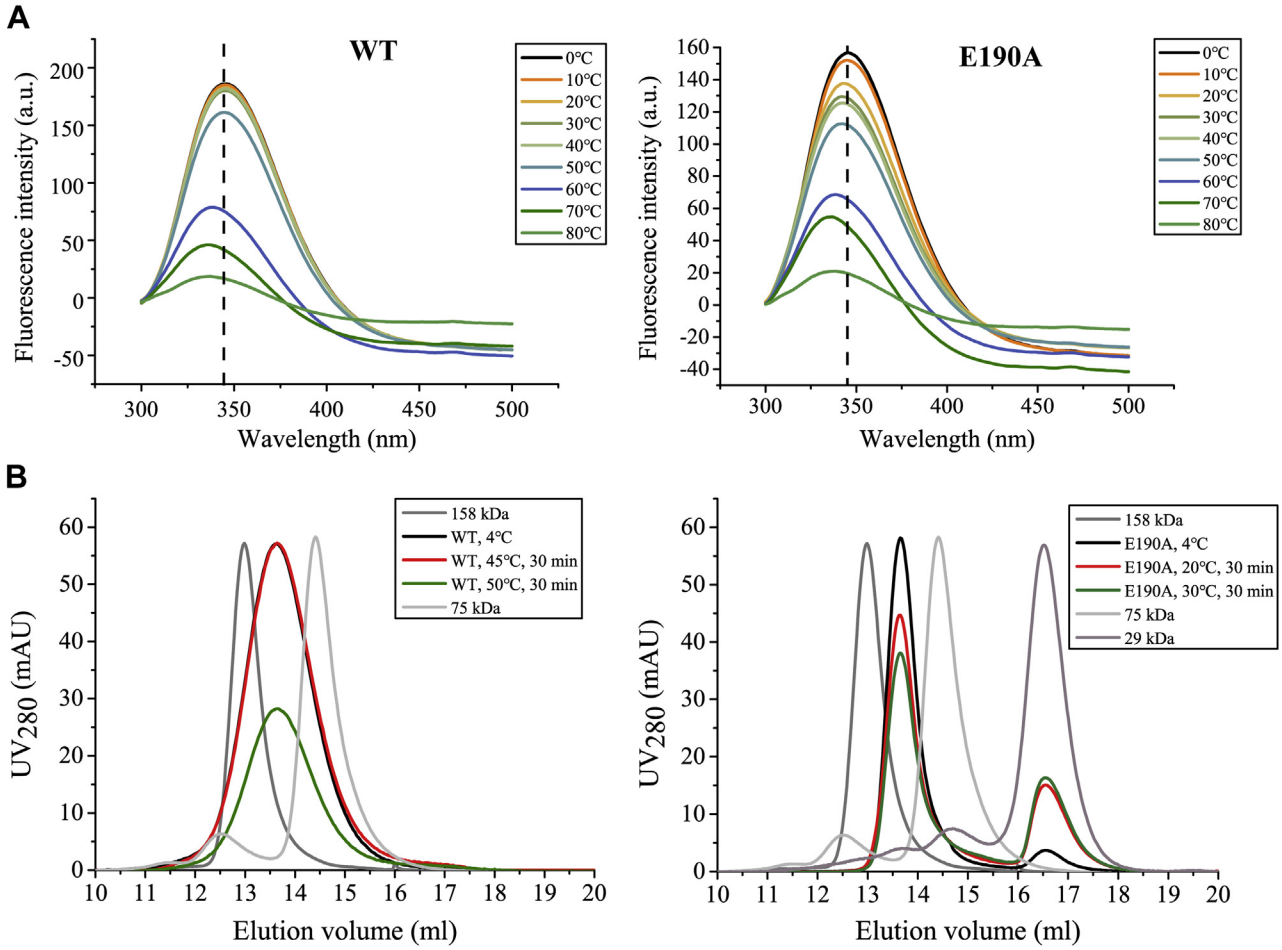

Figure 9. Effect of different temperatures on the structures of WT *Al*AXEase and its mutant E190A. *A*, fluorescence spectra of *Al*AXEase and its mutant E190A after incubation at different temperatures for 1 h. *B*, gel filtration analysis of *Al*AXEase and its mutant E190A after incubation at different temperatures for 30 min. Aldolase (158 kDa), conalbumin (75 kDa), and carbonic anhydrase (29 kDa) were used as protein size markers. The WT *Al*AXEase kept tetramers at all the temperatures measured, whereas a part of the tetramers of mutant E190A were depolymerized to monomers at its optimum temperature of 20 °C. *Al*AXEase, a cold-adapted AcXE from Arctic marine bacterium *Arcticibacterium luteifluviistationis* SM1504[T].

mutant. Different from the reversible active site of *Al*AXEase, the active site of mutant E190A was irreversibly disrupted at a high temperature and thus led to the distortion of the α7 helix upstream of the catalytic loop to a random coil structure (Fig. 10*B*), indicating that the introduced mutation E190A in the catalytic loop makes the region around the active site more susceptible to thermal denaturation than other regions of *Al*AXEase as shown by CD (Fig. 3*C*).

During the MD simulation, we measured the distances between the key residues in the active site to further assess the effect of heat treatment on the active site of *Al*AXEase. At all simulated temperatures, the distance variations between the key residues in the active site were kept at a very small range in *Al*AXEase and mutant E190A except for the distance between the two catalytic residues, Ser32 and His203 (Table 6). For both enzymes, the distances between Ser32 and His203 at 400 K were significantly enlarged compared with those at 280 K, and these distance variations were irreversible when the proteins were cooled from 400 K to 280 K (Table 6). The enlargement of the distance between Ser32 and His203 resulted in the reduction in both activity and substrate affinity of both enzymes at temperatures higher than their respective T_{opt} as indicated in Table 4. Notably, at 280 K, the distance between Ser32 and His203 in mutant E190A (6.5 ± 1.0 Å) is greater than that in the WT (4.3 ± 0.4 Å) (Table 6). Moreover, mutant E190A lost its catalytic activity and substrate-binding ability at a temperature (40 °C) lower than that for the WT (50 °C) (Table 4). All these results suggest that the flexible catalytic loop contributes to the cold-adapted characteristics (high catalytic activity and high substrate affinity at low temperatures) of *Al*AXEase by modulating the distance between the catalytic His203 in this loop and the nucleophilic Ser32, and that the introduced mutation E190A causes a further increase of flexibility in the catalytic loop of *Al*AXEase, leading to an improvement of its cold adaptation.

Discussion

AcXEs play important roles in both marine and terrestrial xylan degradation and recycling (1). AcXEs, dominated by SGNH-type enzymes, are distributed in nine CE families in the CAZy database (3) in addition to the recently discovered Axe2 family (4, 5). Compared with the extensive study on terrestrial mesophilic/thermophilic AcXEs, study on marine cold-adapted AcXEs is still scarce. Until now, owing to the lack of

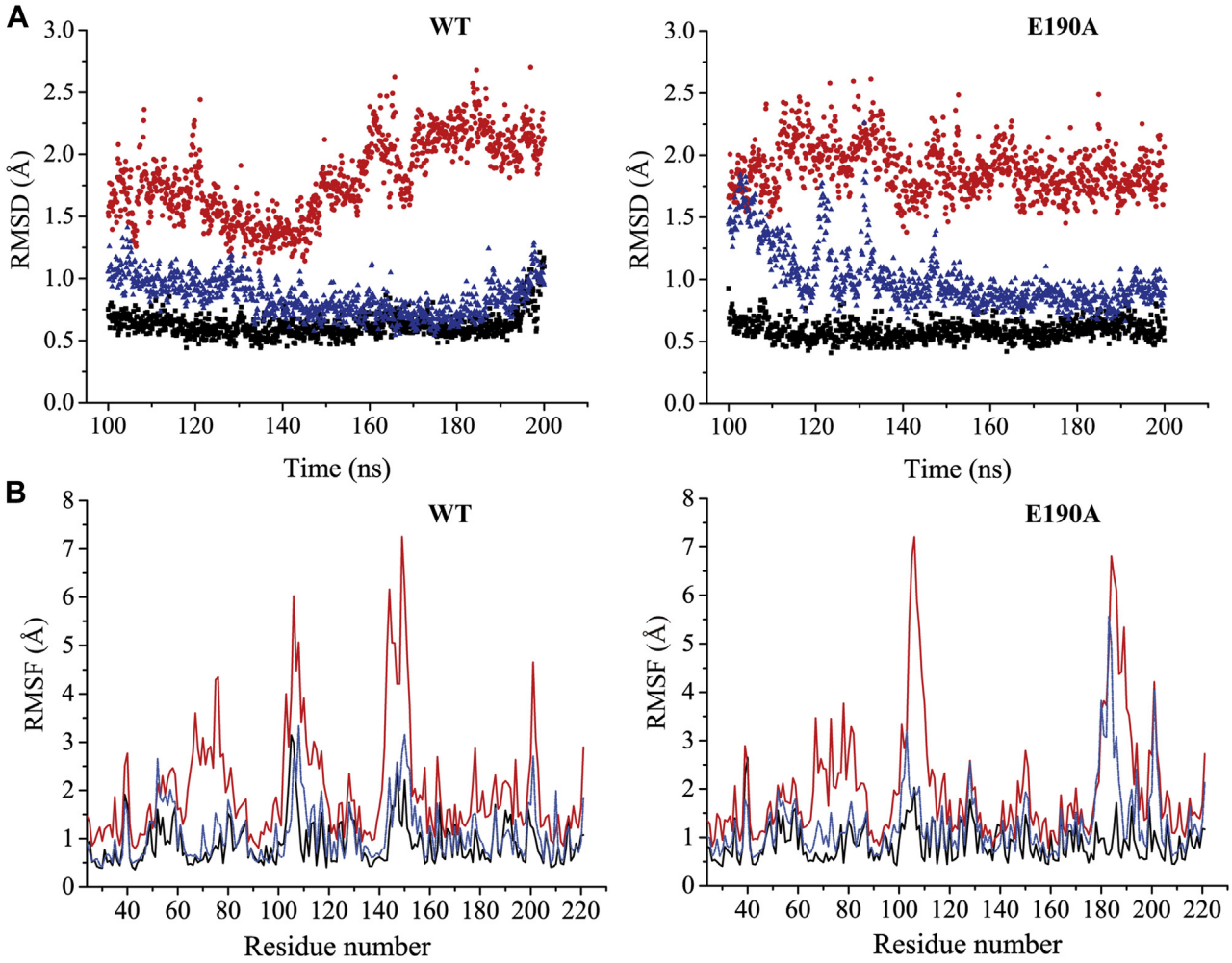

Figure 10. MD simulations of *Al*AXEase and its mutant E190A at different temperatures. *A*, the backbone RMSD values of the MD simulations for *Al*AXEase and its mutant E190A. RMSD values at 280 K and 400 K and that from 400 K back to 280 K are shown in *black*, *red*, and *blue*, respectively. *B*, the residue RMSF values of the MD simulations for *Al*AXEase and its mutant E190A. RMSF values at 280 K and 400 K and that from 400 K back to 280 K are shown in *black*, *red*, and *blue*, respectively. *Al*AXEase, a cold-adapted AcXE from Arctic marine bacterium *Arcticibacterium luteifluviistationis* SM1504^T; RMSF, root mean square fluctuation.

structural information, the cold adaption mechanisms for SGNH-type AcXEs are still unknown. In this study, a novel cold-adapted AcXE, *Al*AXEase, was characterized from the Arctic marine bacterium *A. luteifluviistationis* SM1504^T. *Al*AXEase shares low sequence identities (≤24%) with characterized AcXEs, and phylogenetic analysis suggests that *Al*AXEase and its homologs represent a new SGNH-type CE family. *Al*AXEase had the highest activity at 30 °C and displayed high catalytic activity at 0 to 20 °C, showing its cold-adapted character. However, different from other cold-adapted enzymes that are generally thermolabile (34–36), *Al*AXEase has unusual thermostability, with a relatively high T_m value of 56 °C and stable at temperatures up to 50 °C, suggesting that the cold adaption strategy adopted by *Al*AXEase is different from other thermolabile cold-adapted enzymes.

Most cold-adapted enzymes are highly flexible in their overall structures, leading to their high catalytic activity at low temperatures but low thermostability (21). However, a few cold-adapted enzymes are also reported to be locally flexible without compromising the global stability of proteins (23, 24, 37–39). Biochemical and structural analyses suggested that *Al*AXEase has high overall stability but is flexible in the loop containing the catalytic residues Asp200 and His203 because of the reduced stabilizing hydrophobic interactions and increased destabilizing residues asparagine and lysine (Figs. 6 and 7). Further structural and enzyme kinetic analyses of WT *Al*AXEase and its mutant E190A combined with MD simulations at different temperatures revealed that, the flexible catalytic loop contributes to the cold-adapted characteristics of *Al*AXEase by modulating the distance between the catalytic His203 in this loop and the nucleophilic Ser32. The cold-adapted enzymes *Cp*PAH and *Dp*IDH are also reported to be locally flexible around their active sites because of the disrupted hydrogen-bonding abilities for the cofactor BH_4 (23) and the increase in destabilizing residues such as methionine and charged amino acids (24), respectively. Both *Cp*PAH and *Dp*IDH have flexible active sites through increasing flexibilities in noncatalytic residues in their catalytic cavities, which contribute to their cold-adapted characteristics (23, 24).

Table 6
The distances between key residues in the active sites of WT *Al*AXEase and its mutant E190A based on MD simulations

Enzyme	Crystal/MD simulation	Distance (Å)[a]				
		S32 (Cα) - G69 (N)	S32 (Cα) - N98 (N)	S32 (OG) - H203 (NE2)	D200 (OD1) - H203 (ND1)	D200 (OD2) - H203 (ND1)
WT	Crystal[b]	5.0 ± 0.1	9.1 ± 0.1	3.6 ± 0.2	2.6 ± 0.3	3.5 ± 0.2
	280 K	4.7 ± 0.2	8.6 ± 0.6	4.3 ± 0.4	4.3 ± 1.4	4.8 ± 1.7
	400 K	5.7 ± 1.2	7.0 ± 0.5	10.5 ± 2.4	5.5 ± 2.2	5.5 ± 2.2
	400 K back to 280 K	4.3 ± 0.3	6.8 ± 0.3	11.1 ± 1.4	4.3 ± 1.5	4.9 ± 1.3
E190A	Crystal	_[c]	_[c]	_[c]	_[c]	_[c]
	280 K	6.2 ± 0.3	10.1 ± 0.3	6.5 ± 1.0	3.3 ± 0.3	2.9 ± 0.2
	400 K	7.2 ± 1.5	7.4 ± 0.9	9.3 ± 2.1	4.4 ± 2.0	4.4 ± 2.0
	400 K back to 280 K	7.7 ± 0.7	7.5 ± 0.4	8.2 ± 1.1	3.0 ± 0.5	3.3 ± 0.6

Abbreviation: SeMet, selenomethionine.
[a] The corresponding atom/group of a given residue used for distance calculation is shown in parentheses.
[b] The distances were calculated based on the active sites of four chains in the crystal structure of WT *Al*AXEase.
[c] Undetectable.

However, different from *Cp*PAH, *Dp*IDH, and other cold-adapted enzymes (23, 24, 40), the flexible active site of *Al*AXEase comes from the increased flexibilities in the catalytic residues Asp200 and His203 rather than noncatalytic residues. Therefore, the cold adaption mechanism of *Al*AXEase is different from those of other reported cold-adapted enzymes. The flexible active site contributes to the cold adaptation of *Al*AXEase by modulating the distance between the catalytic residues His203 and Ser32. These data indicate that optimization of the flexibility of the catalytic residues is also a strategy for cold adaptation of enzymes.

The marine strain SM1504^T where *Al*AXEase comes from was reported to be cold adapted, growing at temperatures between 4 °C and 30 °C (optimum of 20 °C) (25). The cold adaptation of *Al*AXEase is consistent with the growth characteristics of strain SM1504^T, suggesting that its structural and biochemical properties are optimized to low temperatures. Genomic analysis showed that this strain contains some genes encoding potential xylanases, arabinofuranosidases, and other xylan-degrading enzymes (26). *Al*AXEase could hydrolyze many kinds of acetylated monosaccharides and disaccharides as well as xylan, with acetylated xylopyranose as the optimal substrate, suggesting that *Al*AXEase is likely involved in xylan/xylooligosaccharide degradation together with other xylan-degrading enzymes to provide carbon source and energy for its source strain. Moreover, the cold-adapted characteristics of *Al*AXEase with unusual thermostability may also help its source strain SM1504^T adapt to the cold polar environment.

Experimental procedures

Gene cloning and mutagenesis

Based on blasting analysis, a gene *AlAXEase* encoding a GDSL family lipolytic protein (GenBank Accession No. WP_111370902) was identified from the genome sequence of marine bacterium *A. luteifluviistationis* SM1504^T. *AlAXEase* without the signal peptide sequence was amplified from the genomic DNA of strain SM1504^T, and the amplified fragment was ligated into the vector pET22b. All of the site-directed mutations and the truncated mutations in *Al*AXEase were introduced with the QuikChange mutagenesis kit (41) using plasmid pET22b-*AlAXEase* as the template. All recombinant plasmids were verified by sequencing.

Protein expression and purification

WT *Al*AXEase protein and all mutants were expressed in *E. coli* BL21 (DE3) with the coexpression of the chaperone *gro*ES-*gro*EL. The cells were cultured at 37 °C to an absorbance at 600 nm of 0.6 to 1.0 and then induced by the addition of 1 mM IPTG and 0.5 mg/ml L-arabinose at 20 °C for 16 h. Cells were collected and disrupted by a JN-02C French press (JNBIO) in 50 mM Tris HCl buffer (pH 8.0) containing 100 mM NaCl and 5 mM imidazole. After centrifugation at 15,000*g* for 1 h at 4 °C, the recombinant proteins were first purified by Ni affinity chromatography (Qiagen) and then by ion-exchange chromatography on a SOURCE 15Q column (GE healthcare). The eluted enzyme fractions were further purified by gel filtration chromatography on a Superdex 200 column (GE healthcare) with 10 mM Tris HCl buffer (pH 8.0) containing 100 mM NaCl. The target protein was collected, and the protein concentration was determined by Pierce BCA Protein Assay Kit (Thermo Scientific).

Enzyme activity assay

Esterase activity was measured as described (42). The standard reaction system (1 ml) contained 50 mM Tris HCl buffer (pH 8.0), 0.02 ml of 10 mM *p*NP-acylesters (Sigma), and 0.02 ml enzyme with an appropriate concentration. After incubation at 30 °C for 5 min, the reaction was terminated by the addition of 0.1 ml 20% SDS (w/v). The absorbance of the reaction mixture at 405 nm was measured using a SpectraMax Plus384 microplate spectrophotometer (Molecular Devices). One unit of enzyme (U) is defined as the amount of enzyme required to liberate 1 μmol *p*-nitrophenol per minute.

The CE activity of *Al*AXEase was determined by detecting the release of acetic acid using synthetic substrates 1-napthyl acetate, phenyl acetate, isopropenyl acetate, menthyl acetate, florfenicol, ethyl 2-chlorobenzoate, and ethyl 4-chloro-3-hydroxybutanoate as well as acetylated carbohydrates β-D-galactose pentaacetate, β-D-glucose pentaacetate, sucrose octaacetate, 1,2,3,5-tetra-O-acetyl-D-xylofuranose, 1,2,3,4-tetra-O-acetyl-D-xylopyranose, benzyl β-D-xylobioside

pentaacetate, partially acetylated xylan, and N-acetyl-D-glucosamine. 1-Napthyl acetate, phenyl acetate, β-D-galactose pentaacetate, β-D-glucose pentaacetate, sucrose octaacetate, and N-acetyl-D-glucosamine were purchased from Sigma. Menthyl acetate, florfenicol, ethyl 2-chlorobenzoate, ethyl 4-chloro-3-hydroxybutanoate, and 1,2,3,4-tetra-O-acetyl-D-xylopyranose were purchased from Aladdin. 1,2,3,5-Tetra-O-acetyl-D-xylofuranose and benzyl β-D-xylobioside pentaacetate were purchased from Zzstandard, and the partially acetylated xylan from Megazyme. The standard assay system contained 0.01 ml of 20 mM substrate dissolved in 50 mM Tris-HCl buffer (pH 9.0) containing 40% (v/v) isopropyl alcohol, and 0.01 ml enzyme with appropriate concentration. The reaction took place for 1 h at 30 °C. The release of acetic acid was determined with an Acetic Acid (ACS Analyser Format) Assay Kit (Megazyme, Ireland) according to the manufacturer's instructions. One unit of enzyme activity (U) was defined as the amount of enzyme required to release 1 μmol of acetic acid per minute.

Biochemical characterization of Al*AXEase and its mutants*

By using *p*NPC2 as the substrate, the biochemical characteristics of *Al*AXEase and its mutants were studied. The T_{opt} for *Al*AXEase activity was measured in the temperature range of 0 to 60 °C at pH 8.0. For thermostability assay, the enzyme was incubated at 40 °C, 50 °C, and 60 °C for different periods, and then, the residual activity was measured at 30 °C. The optimum pH of *Al*AXEase was determined at 30 °C in the Britton–Robinson buffers ranging from pH 2.0 to pH 12.0. For pH stability assay, the enzyme was incubated in buffers with a pH range of 2.0 to 12.0 at 0 °C for 1 h, and then, the residual activity was measured at pH 8.0 and 30 °C. The effect of NaCl on *Al*AXEase activity was determined at NaCl concentrations ranging from 0 to 4.8 M. For salt tolerance assay, the enzyme was incubated at 0 °C for 1 h in buffers containing NaCl ranging from 0 to 4.8 M before the residual activity was measured at 30 °C. The effects of metal ions and potential inhibitors on *Al*AXEase activity were examined by the addition of various chemical agents to the reaction mixture.

Enzyme kinetic assays of *Al*AXEase and its mutants were carried out at pH 9.0 (20 mM Hepes) using 1,2,3,4-tetra-O-acetyl-D-xylopyranose at concentrations from 0.5 to 20 mM. Kinetic parameters were calculated by nonlinear regression fit directly to the Michaelis–Menten equation using the Origin9.0 software.

Crystallization, data collection, and structure determination

Crystals suitable for X-ray diffraction were obtained using the hanging-drop vapor-diffusion method. WT *Al*AXEase crystals grew at 18 °C in the buffer containing 0.1 M succinic acid and 15% (w/v) PEG 3350 for 1 week. Selenomethionine-*Al*AXEase crystals grew at 18 °C in the buffer containing 0.2 M potassium thiocyanate, 0.1 M Bis-Tris propane (pH 7.5), and 20% (w/v) PEG 3350 for 1 week. X-ray diffraction data were collected on the BL17U1 beam line at Shanghai Synchrotron Radiation Facility using Area Detector Systems Corporation Quantum 315r. The initial diffraction data sets were processed by the HKL3000 program (43). *Al*AXEase structure was determined by molecular replacement using the SeMet-*Al*AXEase structure as the starting model. The refinement of *Al*AXEase structure was performed using Coot (44) and Phenix (45). All structure figures were processed using PyMOL.

DLS and CD spectroscopy

The DLS experiments of *Al*AXEase protein and its mutants were carried out using DynaPro NanoStar (Wyatt Technology). The protein concentration was 1 mg/ml (10 mM Tris HCl buffer, pH 8.0, 100 mM NaCl). Data analysis was performed with the Dynamics 7.1.0 software.

CD spectra of WT *Al*AXEase and its mutants were recorded at 25 °C on a J-1000 spectropolarimeter (JASCO). All the spectra were collected from 200 to 250 nm at a scanning rate of 200 nm/min with a path length of 0.1 cm. The protein concentration was 0.1 mg/ml. The thermal unfolding curves were recorded using the spectropolarimeter equipped with a CTU-100 temperature control unit (JASCO). The signal was recorded at 222 nm with a bandwidth of 1 nm. The temperature was monitored using an internal sensor, and the heating rate was 1 °C per min. A 0.1-cm path length cell was used. The protein concentration was 0.2 mg/ml.

Fluorescence measurements

Steady-state fluorescence measurements were performed using an FP-6500 spectrofluorometer (JASCO) equipped with a JULABO computer-controlled thermostat. The excitation wavelength was set at 280 nm and the emission wavelengths at 300 to 500 nm, respectively. Both excitation and emission bandwidths were 5 nm. Cuvettes with a 1-cm path length were used. Proteins were at a concentration of ∼0.06 mg/ml in 50 mM Tris HCl buffer (pH 8.0). Fluorescence spectra of *Al*AXEase and its mutants after incubation at different temperatures for 1 h were recorded, respectively.

MD simulations

The MD simulations of WT *Al*AXEase and its mutant E190A were conducted by using software package GROMACS 2019.6 (46), with the force field Amber99sb-ildn (47) adopted. The enzyme structure was first placed into the center of a virtual cubic box with side length of 7.57 nm for WT and 7.36 nm for E190A and then solvated with 12,613 and 11,875 TIP3P water molecule model for WT and E190A, respectively. Sodium ions were added to the virtual water box as counter ions to neutralize the negative charge of the entire system (5 Na^+ for WT and 4 Na^+ for E190A). Energy minimization of the system was conducted using the steepest descent algorithm for 10,000 steps, followed by a 1-ns equilibration simulation with harmonic position restraints on the heavy atoms of protein to equilibrate the solvent molecules around the protein at the desired temperature. Subsequently, the simulation was performed for 200 ns at the target temperature without any position restraints. All simulations were performed under the NPT ensemble with periodic boundary conditions and a time step of 2 fs. The system was kept at a certain temperature using the v-rescale method, as well as the pressure was kept at 1 bar

using the Parrinello–Rahman method. The temperature of the simulation was set to 280 K and 400 K. The final frame of the simulation performed under 400 K was used as the initial conformation to conduct another simulation under 280 K. According to the plot of the RMSD, trajectories that reached the equilibrium state (100 ns–200 ns) were used for analysis. The dynamics changes of the root mean square fluctuation values and the secondary structure against time were analyzed by using the built-in tools of GROMACS.

Data availability

The atomic coordinates and structure factors of *Al*AXEase have been deposited in the PDB with accession code 7DDY.

Supporting information—This article contains supporting information.

Acknowledgments—We thank the staffs from BL17U1 and BL18U1 beamlines of the National Facility for Protein Science Shanghai and Shanghai Synchrotron Radiation Facility, for assistance during data collection.
We would like to thank Jingyao Qu, Jing Zhu, and Zhifeng Li from State Key laboratory of Microbial Technology of Shandong University for help and guidance in dynamic light scattering.
This work was supported by the National Key Research and Development Program of China (2018YFC1406700, 2018YFC1406704), the National Natural Science Foundation of China (31630012, U1706207, 91851205, 91751101, 41906195, and 41676180), Major Scientific and Technological Innovation Project (MSTIP) of Shandong Province (2019JZZY010817), the Program of Shandong for Taishan Scholars (tspd20181203), and the Young Scholars Program of Shandong University (2017WLJH57).

Author contributions—Y. Z., W.-X. J., and J.-P. W. methodology; Y. Z. writing–original draft; H.-T. D., H.-Y. C., and C.-Y. L. software; H.-T. D., H.-Y. C., and C.-Y. L. formal analysis; X. Z., F. H., X.-Y. Z., X.-L. C., Y.-Z. Z., and P.-Y. L. project administration; X.-L. C. and P.-Y. L. writing–review and editing; Y.-Z. Z. and P.-Y. L. funding acquisition.

Conflict of interest—The authors declare that they have no conflicts of interest with the contents of this article.

Abbreviations—The abbreviations used are: AcXEs, acetyl xylan esterases; *Al*AXEase, a cold-adapted AcXE from Arctic marine bacterium *Arcticibacterium luteifluviistationis* SM1504^{T}; CEs, carbohydrate esterases; *Cp*PAH, phenylalanine hydroxylase from *Colwellia psychrerythraea* 34H; DLS, dynamic light scattering; *Dp*IDH, isocitrate dehydrogenase from *Desulfotalea psychrophila*; PDB, Protein Data Bank; *p*NPC2, *p*-nitrophenyl acetate; SeMet, selenomethionine; T_{opt}, optimum temperature.

References

1. Adesioye, F. A., Makhalanyane, T. P., Biely, P., and Cowan, D. A. (2016) Phylogeny, classification and metagenomic bioprospecting of microbial acetyl xylan esterases. *Enzyme Microb. Technol.* **93-94**, 79–91
2. Komiya, D., Hori, A., Ishida, T., Igarashi, K., Samejima, M., Koseki, T., and Fushinobu, S. (2017) Crystal structure and substrate specificity modification of acetyl xylan esterase from *Aspergillus luchuensis*. *Appl. Environ. Microbiol.* **83**, e01251-17
3. Lombard, V., Golaconda Ramulu, H., Drula, E., Coutinho, P. M., and Henrissat, B. (2014) The carbohydrate-active enzymes database (CAZy) in 2013. *Nucleic Acids Res.* **42**, D490–D495
4. Alalouf, O., Balazs, Y., Volkinshtein, M., Grimpel, Y., Shoham, G., and Shoham, Y. (2011) A new family of carbohydrate esterases is represented by a GDSL hydrolase/acetylxylan esterase from *Geobacillus stearothermophilus*. *J. Biol. Chem.* **286**, 41993–42001
5. Soni, S., Sathe, S. S., Odaneth, A. A., Lali, A. M., and Chandrayan, S. K. (2017) SGNH hydrolase-type esterase domain containing Cbes-AcXE2: A novel and thermostable acetyl xylan esterase from *Caldicellulosiruptor bescii*. *Extremophiles* **21**, 687–697
6. Koutaniemi, S., van Gool, M. P., Juvonen, M., Jokela, J., Hinz, S. W., Schols, H. A., and Tenkanen, M. (2013) Distinct roles of carbohydrate esterase family CE16 acetyl esterases and polymer-acting acetyl xylan esterases in xylan deacetylation. *J. Biotechnol.* **168**, 684–692
7. Tian, Q., Song, P., Jiang, L., Li, S., and Huang, H. (2014) A novel cephalosporin deacetylating acetyl xylan esterase from *Bacillus subtilis* with high activity toward cephalosporin C and 7-aminocephalosporanic acid. *Appl. Microbiol. Biotechnol.* **98**, 2081–2089
8. Park, S. H., Yoo, W., Lee, C. W., Jeong, C. S., Shin, S. C., Kim, H. W., Park, H., Kim, K. K., Kim, T. D., and Lee, J. H. (2018) Crystal structure and functional characterization of a cold-active acetyl xylan esterase (*Pb*AcE) from psychrophilic soil microbe *Paenibacillus* sp. *PLoS One* **13**, e0206260
9. Razeq, F. M., Jurak, E., Stogios, P. J., Yan, R., Tenkanen, M., Kabel, M. A., Wang, W., and Master, E. R. (2018) A novel acetyl xylan esterase enabling complete deacetylation of substituted xylans. *Biotechnol. Biofuels* **11**, 74
10. Akoh, C. C., Lee, G. C., Liaw, Y. C., Huang, T. H., and Shaw, J. F. (2004) GDSL family of serine esterases/lipases. *Prog. Lipid Res.* **43**, 534–552
11. Li, J., Derewenda, U., Dauter, Z., Smith, S., and Derewenda, Z. S. (2000) Crystal structure of the *Escherichia coli* thioesterase II, a homolog of the human Nef binding enzyme. *Nat. Struct. Biol.* **7**, 555–559
12. Molgaard, A., Kauppinen, S., and Larsen, S. (2000) Rhamnogalacturonan acetylesterase elucidates the structure and function of a new family of hydrolases. *Structure* **8**, 373–383
13. Lescic Asler, I., Stefanic, Z., Marsavelski, A., Vianello, R., and Kojic-Prodic, B. (2017) Catalytic dyad in the SGNH hydrolase superfamily: In-depth insight into structural parameters tuning the catalytic process of extracellular lipase from *Streptomyces rimosus*. *ACS Chem. Biol.* **12**, 1928–1936
14. Correia, M. A. S., Prates, J. A. M., Bras, J., Fontes, C. M. G. A., Newman, J. A., Lewis, R. J., Gilbert, H. J., and Flint, J. E. (2008) Crystal structure of a cellulosomal family 3 carbohydrate esterase from *Clostridium thermocellum* provides insights into the mechanism of substrate recognition. *J. Mol. Biol.* **379**, 64–72
15. Lansky, S., Alalouf, O., Solomon, H. V., Alhassid, A., Govada, L., Chayen, N. E., Belrhali, H., Shoham, Y., and Shoham, G. (2014) A unique octameric structure of Axe2, an intracellular acetyl-xylooligosaccharide esterase from *Geobacillus stearothermophilus*. *Acta Crystallogr. D Biol. Crystallogr.* **70**, 261–278
16. Till, M., Goldstone, D. C., Attwood, G. T., Moon, C. D., Kelly, W. J., and Arcus, V. L. (2013) Structure and function of an acetyl xylan esterase (Est2A) from the rumen bacterium *Butyrivibrio proteoclasticus*. *Proteins* **81**, 911–917
17. Martinez-Martinez, I., Navarro-Fernandez, J., Daniel Lozada-Ramirez, J., Garcia-Carmona, F., and Sanchez-Ferrer, A. (2008) YesT: A new rhamnogalacturonan acetyl esterase from *Bacillus subtilis*. *Proteins* **71**, 379–388
18. Blum, D. L., Li, X. L., Chen, H. Z., and Ljungdahl, L. G. (1999) Characterization of an acetyl xylan esterase from the anaerobic fungus *Orpinomyces* sp. strain PC-2. *Appl. Environ. Microbiol.* **65**, 3990–3995
19. Nagel, Z. D., Cun, S., and Klinman, J. P. (2013) Identification of a long-range protein network that modulates active site dynamics in extremophilic alcohol dehydrogenases. *J. Biol. Chem.* **288**, 14087–14097
20. Papaleo, E., Riccardi, L., Villa, C., Fantucci, P., and De Gioia, L. (2006) Flexibility and enzymatic cold-adaptation: A comparative molecular

dynamics investigation of the elastase family. *Biochim. Biophys. Acta* **1764**, 1397–1406
21. Siddiqui, K. S., and Cavicchioli, R. (2006) Cold-adapted enzymes. *Annu. Rev. Biochem.* **75**, 403–433
22. Xie, B. B., Bian, F., Chen, X. L., He, H. L., Guo, J., Gao, X., Zeng, Y. X., Chen, B., Zhou, B. C., and Zhang, Y. Z. (2009) Cold adaptation of zinc metalloproteases in the thermolysin family from deep sea and Arctic sea ice bacteria revealed by catalytic and structural properties and molecular dynamics new insights into relationship between conformational flexibility and hydrogen bonding. *J. Biol. Chem.* **284**, 9257–9269
23. Leiros, H. K., Pey, A. L., Innselset, M., Moe, E., Leiros, I., Steen, I. H., and Martinez, A. (2007) Structure of phenylalanine hydroxylase from *Colwellia psychrerythraea* 34H, a monomeric cold active enzyme with local flexibility around the active site and high overall stability. *J. Biol. Chem.* **282**, 21973–21986
24. Fedoy, A. E., Yang, N., Martinez, A., Leiros, H. K., and Steen, I. H. (2007) Structural and functional properties of isocitrate dehydrogenase from the psychrophilic bacterium *Desulfotalea psychrophila* reveal a cold-active enzyme with an unusual high thermal stability. *J. Mol. Biol.* **372**, 130–149
25. Li, D. D., Peng, M., Wang, N., Wang, X. J., Zhang, X. Y., Chen, X. L., Su, H. N., Zhang, Y. Z., and Shi, M. (2017) *Arcticibacterium luteifluviistationis* gen. nov., sp. nov., isolated from Arctic seawater. *Int. J. Syst. Evol. Microbiol.* **67**, 664–669
26. Li, Y., Guo, X. H., Dang, Y. R., Sun, L. L., Zhang, X. Y., Chen, X. L., Qin, Q. L., and Wang, P. (2018) Complete genome sequence of *Arcticibacterium luteifluviistationis* SM1504^{T}, a cytophagaceae bacterium isolated from Arctic surface seawater. *Stand Genomic Sci.* **13**, 33
27. Pfeffer, J. M., Weadge, J. T., and Clarke, A. J. (2013) Mechanism of action of *Neisseria gonorrhoeae* O-acetylpeptidoglycan esterase, an SGNH serine esterase. *J. Biol. Chem.* **288**, 2605–2613
28. Tang, M. A., Motoshima, H., and Watanabe, K. (2012) Fluorescence studies on the stability, flexibility and substrate-induced conformational changes of acetate kinases from psychrophilic and mesophilic bacteria. *Protein J.* **31**, 337–344
29. Struvay, C., and Feller, G. (2012) Optimization to low temperature activity in psychrophilic enzymes. *Int. J. Mol. Sci.* **13**, 11643–11665
30. Sanchez-Ruiz, J. M., and Makhatadze, G. I. (2001) To charge or not to charge? *Trends Biotechnol.* **19**, 132–135
31. Tanaka, Y., Tsumoto, K., Yasutake, Y., Umetsu, M., Yao, M., Fukada, H., Tanaka, I., and Kumagai, I. (2004) How oligomerization contributes to the thermostability of an Archaeon protein. Protein L-isoaspartyl-O-methyltransferase from *Sulfolobus tokodaii*. *J. Biol. Chem.* **279**, 32957–32967
32. Ogasahara, K., Ishida, M., and Yutani, K. (2003) Stimulated interaction between alpha and beta subunits of tryptophan synthase from hyperthermophile enhances its thermal stability. *J. Biol. Chem.* **278**, 8922–8928
33. Martinez, L. (2015) Automatic identification of mobile and rigid substructures in molecular dynamics simulations and fractional structural fluctuation analysis. *PLoS One* **10**, e0119264
34. Zhao, F., Cao, H. Y., Zhao, L. S., Zhang, Y., Li, C. Y., Zhang, Y. Z., Li, P. Y., Wang, P., and Chen, X. L. (2019) A novel subfamily of endo-beta-1,4-glucanases in glycoside hydrolase family 10. *Appl. Environ. Microbiol.* **85**, e01029-19
35. Rutkiewicz, M., Bujacz, A., and Bujacz, G. (2019) Structural features of cold-adapted dimeric GH2 beta-D-galactosidase from *Arthrobacter* sp. 32cB. *Biochim. Biophys. Acta Proteins Proteom.* **1867**, 776–786
36. Lee, C. W., Kwon, S., Park, S. H., Kim, B. Y., Yoo, W., Ryu, B. H., Kim, H. W., Shin, S. C., Kim, S., Park, H., Kim, T. D., and Lee, J. H. (2017) Crystal structure and functional characterization of an esterase (EaEST) from *Exiguobacterium antarcticum*. *PLoS One* **12**, e0169540
37. Le, L. T. H. L., Yoo, W., Jeon, S., Lee, C., and Kim, T. D. (2020) Biodiesel and flavor compound production using a novel promiscuous cold-adapted SGNH-type lipase (HaSGNH1) from the psychrophilic bacterium *Halocynthiibacter arcticus*. *Biotechnol. Biofuels* **13**, 55
38. Lian, K., Leiros, H. K., and Moe, E. (2015) MutT from the fish pathogen *Aliivibrio salmonicida* is a cold-active nucleotide-pool sanitization enzyme with unexpectedly high thermostability. *FEBS Open Bio* **5**, 107–116
39. Yang, G., De Santi, C., de Pascale, D., Pucciarelli, S., Pucciarelli, S., and Miceli, C. (2013) Characterization of the first eukaryotic cold-adapted patatin-like phospholipase from the psychrophilic *Euplotes focardii*: Identification of putative determinants of thermal-adaptation by comparison with the homologous protein from the mesophilic *Euplotes crassus*. *Biochimie* **95**, 1795–1806
40. Kulakova, L., Galkin, A., Nakayama, T., Nishino, T., and Esaki, N. (2004) Cold-active esterase from *Psychrobacter* sp. Ant300: Gene cloning, characterization, and the effects of Gly→Pro substitution near the active site on its catalytic activity and stability. *Biochim. Biophys. Acta* **1696**, 59–65
41. Liu, H., and Naismith, J. H. (2008) An efficient one-step site-directed deletion, insertion, single and multiple-site plasmid mutagenesis protocol. *BMC Biotechnol.* **8**, 91
42. Li, P. Y., Ji, P., Li, C. Y., Zhang, Y., Wang, G. L., Zhang, X. Y., Xie, B. B., Qin, Q. L., Chen, X. L., Zhou, B. C., and Zhang, Y. Z. (2014) Structural basis for dimerization and catalysis of a novel esterase from the GTSAG motif subfamily of the bacterial hormone-sensitive lipase family. *J. Biol. Chem.* **289**, 19031–19041
43. Minor, W., Cymborowski, M., Otwinowski, Z., and Chruszcz, M. (2006) HKL-3000: The integration of data reduction and structure solution–from diffraction images to an initial model in minutes. *Acta Crystallogr. D Biol. Crystallogr.* **62**, 859–866
44. Emsley, P., and Cowtan, K. (2004) Coot: Model-building tools for molecular graphics. *Acta Crystallogr. D Biol. Crystallogr.* **60**, 2126–2132
45. Adams, P. D., Grosse-Kunstleve, R. W., Hung, L. W., Ioerger, T. R., McCoy, A. J., Moriarty, N. W., Read, R. J., Sacchettini, J. C., Sauter, N. K., and Terwilliger, T. C. (2002) PHENIX: Building new software for automated crystallographic structure determination. *Acta Crystallogr. D Biol. Crystallogr.* **58**, 1948–1954
46. Abraham, M. J., Murtola, T., Schulz, R., Páll, S., Smith, J. C., Hess, B., and Lindahl, E. (2015) GROMACS: High performance molecular simulations through multi-level parallelism from laptops to supercomputers. *SoftwareX* **1-2**, 19–25
47. Hornak, V., Abel, R., Okur, A., Strockbine, B., Roitberg, A., and Simmerling, C. (2006) Comparison of multiple Amber force fields and development of improved protein backbone parameters. *Proteins* **65**, 712–725
48. Li, P. Y., Chen, X. L., Ji, P., Li, C. Y., Wang, P., Zhang, Y., Xie, B. B., Qin, Q. L., Su, H. N., Zhou, B. C., Zhang, Y. Z., and Zhang, X. Y. (2015) Interdomain hydrophobic interactions modulate the thermostability of microbial esterases from the hormone-sensitive lipase family. *J. Biol. Chem.* **290**, 11188–11198
49. Wang, P., Chen, X. L., Li, C. Y., Gao, X., Zhu, D. Y., Xie, B. B., Qin, Q. L., Zhang, X. Y., Su, H. N., Zhou, B. C., Xun, L. Y., and Zhang, Y. Z. (2015) Structural and molecular basis for the novel catalytic mechanism and evolution of DddP, an abundant peptidase-like bacterial dimethylsulfoniopropionate lyase: A new enzyme from an old fold. *Mol. Microbiol.* **98**, 289–301